

POLITECNICO
MILANO 1863

SCUOLA DI INGEGNERIA INDUSTRIALE
E DELL'INFORMAZIONE

Assisted bimanual rehabilitation using IMU-based control: an early study

Tesi di Laurea Magistrale in
Biomedical Engineering - Ingegneria Biomedica

Author: **Giulia Liliana Bonesi**

Student ID: 249979
Advisor: Prof. Marta Gandolla
Academic Year: 2025-2026

Abstract

Stroke frequently causes persistent upper-limb impairment, limiting independence in activities of daily living. Since many functional tasks require coordinated use of both arms, bimanual rehabilitation represents a promising strategy to promote motor recovery.

This thesis develops an IMU-based master–slave framework for assisted bimanual upper-limb rehabilitation. The movement of the non-affected arm is acquired using three NGIMU sensors positioned on the trunk, upper arm and forearm, processed in real time, and used to reconstruct upper-limb kinematics and generate a mirrored contralateral reference for future exoskeleton control.

The developed pipeline was preliminarily validated through isolated joint movements, functional reaching tasks and postural tests. Performance was assessed using range of motion, cross-talk, hand trajectory, movement duration, hand velocity, sagittal-plane distance, residual angular variation and acquisition rate.

Results support the feasibility of the proposed approach and show repeatable three-dimensional motion reconstruction, while also identifying limitations related mainly to calibration and joint-angle decoupling. The system therefore provides a technological basis for future integration with a unilateral exoskeleton and subsequent validation in post-stroke rehabilitation.

Keywords: Stroke rehabilitation; Bimanual rehabilitation; Upper-limb rehabilitation; Inertial Measurement Units (IMUs); Master–slave control; Mirror control; Motion tracking.

Abstract in lingua italiana

L'ictus determina frequentemente deficit persistenti dell'arto superiore, con conseguente riduzione dell'autonomia nelle attività della vita quotidiana. Poiché molte azioni funzionali richiedono l'impiego coordinato di entrambi gli arti, la riabilitazione bimanuale rappresenta una strategia promettente per favorire il recupero motorio. La presente tesi sviluppa un framework master–slave basato su IMU per la riabilitazione bimanuale assistita dell'arto superiore. Il movimento dell'arto non affetto viene acquisito mediante tre sensori NGIMU posizionati su tronco, braccio e avambraccio, elaborato in tempo reale e utilizzato per ricostruire la cinematica dell'arto e generare un riferimento speculare controlaterale destinato al futuro controllo di un esoscheletro.

La pipeline è stata validata preliminarmente mediante movimenti articolari isolati, task funzionali di reaching e test posturali. Le prestazioni sono state valutate attraverso range of motion, cross-talk, traiettoria della mano, durata del movimento, velocità, distanza dal piano sagittale, variazione angolare residua e frequenza di acquisizione.

I risultati supportano la fattibilità dell'approccio e mostrano una ricostruzione tridimensionale sufficientemente ripetibile, evidenziando al contempo criticità legate soprattutto alla calibrazione e al disaccoppiamento articolare. Il sistema costituisce quindi una base tecnologica per la futura integrazione con un esoscheletro unilaterale e per successive validazioni in ambito post-ictus.

Parole chiave: Riabilitazione post-ictus; Riabilitazione bimanuale; Riabilitazione dell'arto superiore; Unità di misura inerziali (IMU); Controllo master–slave; Controllo mirror; Tracciamento del movimento.

Contents

Abstract **i**

Abstract in lingua italiana **iii**

Contents **v**

1 Introduction **1**
1.1 Stroke and clinical context 1
1.2 Bimanual therapy and motivation 2

2 State of the art **4**
2.1 Control system 4
2.2 Sensor integration 7
2.3 Coordination patterns 10
2.4 Use case and exercise 13
2.5 Literature gap 16
2.6 Aim of the study 17

3 Materials and methods **19**
3.1 Materials 19
3.2 Methods: NGIMU simulation 21
3.2.1 Conventions used and modifications 22
3.2.2 3D simulation 26
3.3 Testing protocol 28

4 Results **39**
4.1 Analyzed sample 39
4.2 Angular agreement 40
4.3 Angular repetability 43
4.4 Wrist trajectories and repeatability in A2 44

4.5 Contacts heights in B1 46
4.6 Intra-patients analisys 47

5 Discussion **49**
5.1 Basis of bimanual simulation 49
5.2 Elbow reconstruction and differences from OpenCap 50
5.3 Spatial reconstruction: repeatability and limitations 51

6 Conclusion **53**
6.1 Main findings 53
6.2 Future development 54

Bibliography **56**

A Appendix A **58**
A.1 Test A1.1 59
A.2 Test A1.2 61
A.3 Test A1.3 63
A.4 Test A2 65
A.5 Test B1 68

List of Figures **70**

List of Tables **72**

1 | Introduction

Stroke is one of the leading causes of long-term mortality and disability worldwide and therefore represents a significant clinical and social health problem [5, 10]. The neurological consequences of a cerebrovascular accident can lead to varying degrees of motor, sensory, and cognitive impairment, significantly affecting individual autonomy and quality of life. Among the most frequent consequences is the impairment of the upper limb, which can substantially limit the patient's ability to perform functional activities and tasks of daily living.

Recovery of upper limb function is therefore one of the primary goals of post-stroke neurorehabilitation. In this context, modern rehabilitation approaches aim to promote high-intensity exercise, repetition of movements, active participation of the patient, and the execution of functionally significant tasks. The availability of robotic technologies and motion acquisition systems also offers the possibility of making treatment more repeatable, quantitative, and adaptable to the characteristics of the individual patient.

This thesis is part of this context and proposes the preliminary development of a bimanual-assisted rehabilitation paradigm, in which voluntary movement of the unaffected limb is acquired using inertial sensors and used as a kinematic reference for the generation of assisted movement of the affected limb using a single arm exoskeleton for the upper limb. The main idea behind this approach is to integrate the principles of bimanual therapy, rehabilitation robotics, and wearable sensing within a mirror/master–slave control strategy.

1.1. Stroke and clinical context

Stroke is an acute neurological event that occurs when blood flow to a specific area of the brain is reduced or interrupted. It can be ischemic, due to occlusion of a blood vessel, or hemorrhagic, due to vessel rupture. In both cases, the reduced supply of oxygen and nutrients leads to neuronal damage, whose severity and location influence the resulting clinical and functional impairments. [5, 10].

Despite advances in prevention and treatment of the acute phase, stroke remains a lead-

ing cause of acquired disability in adults [5, 10]. Motor consequences frequently include muscle weakness, reduced voluntary motor control, alterations in tone, and difficulty coordinating multi-joint movements. In particular, hemiparesis can compromise the ability to control the upper limb contralateral to the lesion and interfere with unimanual actions and those requiring coordinated participation of both limbs.
Impairment of the upper limb takes on particular clinical relevance because numerous activities of daily living require the ability to reach, manipulate, and transport objects. Kiper et al. [13] highlight how upper limb motor deficits can persist even after the acute event and negatively impact autonomy in Activities of Daily Living (ADL). The same authors also emphasize the role of central nervous system reorganization and intensive stimulation in the post-stroke motor recovery process.
Functional recovery should therefore not be interpreted exclusively as the restoration of individual joint movements, but as the recovery of the ability to effectively use the limb in goal-oriented actions. This consideration is particularly important for the upper limb, characterized by complex kinematics and the need to coordinate different joints and body segments during the execution of functional activities.
To promote recovery, rehabilitation protocols must therefore create conditions that allow the patient to perform a large number of meaningful and repeatable movements while maintaining adequate motor involvement. In this context, rehabilitation robotics represents a potentially useful tool to support movement and increase the amount of available practice, without, however, replacing the neurophysiological and functional principles on which treatment must be built.

1.2. Bimanual therapy and motivation

A limitation of exclusively unimanual rehabilitation derive from the fact that many activities of daily living require the coordinated use of both limbs. Dressing, eating or manipulating a complex object are examples of tasks in which the two limbs must be organized within the same functional action. Bimanual therapy is based on the simultaneous or coordinated execution of movements of the affected and unaffected limbs. The neurophysiological motivation consists in the involvement of both cerebral hemispheres and the possible modulation of interhemispheric activation and inhibition mechanisms. The relevance of this approach is not exclusively neurophysiological, but also functional. Bilateral training allows the movement of the paretic limb to be placed in a context more similar to that of daily activities. Furthermore, the two limbs do not necessarily have to perform identical movements: bimanual actions can be symmetrical or asymmetrical and cooperative, with different roles for each hand [11]. Interest in bimanual rehabilitation

has been strengthened by the possibility of implementing these principles through robotic devices. A study on chronic post-stroke patients,[11] showed that learning an asymmetrical bimanual task mediated by a robotic interface was possible, although performance was influenced by the degree of motor impairment.
Interesting results also emerge from clinical studies on bilateral robot-assisted training. Tang et al. [19] observed, after a bilateral protocol, an improvement in daily living skills and an increase in functional connectivity between the two hemispheres, although they did not demonstrate a clear superiority for motor outcomes compared to conventional therapy. A particularly relevant approach for this thesis is represented by the mirror-guided modality, in which the movement of the unaffected limb is used directly as a reference for assistance of the paretic limb. Ma et al. [17] implemented this paradigm at the hand level using a sensorized glove on the unaffected limb and an exoskeleton applied to the paretic hand. The signals acquired by the glove were processed by the control system and transferred to the exoskeleton, allowing the movement to be reproduced according to a mirror-symmetric pattern.
These results suggest that using the movement of the unaffected limb as a source of information for robotic assistance represents a particularly interesting paradigm. The reference movement is not defined exclusively through pre-programmed trajectories, but can derive directly from the subject's voluntary action. This principle allows us to imagine the unaffected side as the master and the assisted side as the slave, introducing a direct relationship between motor intention, the subject's physiological movement, and robotic assistance.
This thesis develops this approach: the motion of the master side is acquired using inertial measurement units positioned on the body segments and reconstructed through a dedicated kinematic pipeline. The resulting reference constitutes the basis for generating a mirrored contralateral motion, intended for subsequent integration with a unilateral exoskeleton.
The goal is therefore not simply to assist a single movement of the paretic limb, but to establish the necessary architecture for a training model in which voluntary action of the unaffected limb, wearable acquisition, and robotic assistance of the paretic limb are integrated within the same bimanual task. The definition of the technologies control strategies and coordination patterns available in the literature is explored in the next chapter.

2 | State of the art

This chapter organizes the state of the art according to four dimensions directly related to the paradigm developed in the thesis: control system, sensory integration, coordination pattern, and choice of use cases and exercises. This organization allows us to gradually move from the description of existing solutions to the definition of the literature gap and, finally, the specific objective of the work.

2.1. Control system

In robotic systems for neurorehabilitation, the control system determines the mode in which the device dictates, assists, or modulates the user's movement. Bilateral upper limb robots have implemented very different modes, including passive, active-assisted, active-resisted, synchronized, and master–slave movements [18].
Generally speaking, control architectures can be categorized along a continuum ranging from preprogrammed control, in which the trajectory is defined by the system, to adaptive and human-in-the-loop control, in which the reference is updated based on kinematic, kinetic, or bioelectrical signals. More recent sensor-driven strategies include force control, assist-as-needed, human-in-the-loop, gravitational compensation, and predictive approaches; the choice depends on the level of impairment, the degree of voluntary participation required, and the type of task [12].

Passive control and predefined trajectories

In passive control, the robot generates joint movement without requiring sufficient motor output from the user. This mode can be useful in the initial stages or in subjects with severe impairment, in which mobilization allows repeated movements within a defined range. The main limitation is reduced active participation: excessive imposition of the trajectory can decrease voluntary contribution and make training less representative of the patient's spontaneous motor strategies. For this reason, many devices combine the passive mode with progressively more interactive modes [11, 12, 18].

Mirror and master–slave control

The mirror/master–slave paradigm is particularly relevant in patients with unilateral impairment. In this configuration, the less impaired limb, or a device associated with it, constitutes the master side and generates the movement reference; the slave side applied to the paretic limb reproduces or assists a corresponding movement. The conceptual advantage is that the trajectory does not derive exclusively from a sequence predefined by the programmer or therapist, but can be generated directly by the subject's voluntary movement.

A distal example is the system proposed by Triwiyanto et al. that has developed a hand exoskeleton consisting of a master and a slave section: five IMUs placed on the fingers of the non-paretic hand provide the angles transmitted wirelessly to the paretic side, where servomotors reproduce the movement [20]. The principle has been extended to more proximal segments by Kwok and Yu, who implemented a master–slave strategy at the joint level in a bilateral underactuated exoskeleton, using the trajectories measured on the master side as the desired reference for impedance control of the slave side [14].

More recent literature also proposes forms of mirror control that are not rigidly one-to-one. Chen et al. combine the kinematics of the healthy limb with sEMG of the affected limb and generate a variable mirroring coefficient inserted into an admittance control, with the aim of adapting the trajectory to the patient's residual capacities [7]. This evolution highlights an important distinction: mirror control can be implemented as a direct geometric replica or as an adaptive reference, keeping the unaffected side as the primary source of information.

Active-assisted (AAN) control

In active-assisted control, the subject initiates or contributes to the movement, while the robot provides the support needed to complete the trajectory. Assist-as-needed strategies represent a more adaptive variant: assistance is reduced when the patient is able to perform the task autonomously and increased when performance deviates from the target. From a rehabilitation perspective, this approach aims to avoid excessive dependence on the device and to preserve motor involvement. Contemporary reviews place assistance-as needed and adaptive control among central strategies for personalizing the amount of support [12].

EMG-triggered control

EMG-triggered strategies use electromyographic activity as an indicator of voluntary intention. Exceeding a threshold or recognizing a muscle pattern can activate stimulation or robotic assistance. In a classic study, Cauraugh and Kim combined bilateral movements with EMG-triggered neuromuscular stimulation, observing improvements in wrist and finger functional abilities compared to comparator protocols [6]. This approach is particularly interesting because it requires an active motor attempt, but presents critical issues related to the variability of the signal, the positioning of the electrodes, and the need for preprocessing and individual thresholds.

Impedance, admittance and gravitational compensation control

Impedance and admittance strategies regulate the relationship between motion and interaction forces, allowing for more compliant behavior than simple position imposition. In impedance control, the deviation between the desired and actual configuration generates a corrective torque modulated by stiffness and damping; in admittance control, however, a measured force or torque is converted into a motion variable. These architectures are particularly suited to physical human-robot interaction because they allow for modulation of transparency and assistance [12].
Little et al. showed an example of integrating inertial sensing unit and assistance control in a soft exosuit: shoulder and elbow angles estimated by the IMU are employed within a gravitational compensation model, whose outer loop uses admittance logic to generate the velocity reference [15]. This study demonstrates how the IMU can be used not only to describe motion a posteriori, but as a variable directly functional to modulate assistance.

Cooperative control

In cooperative systems, the outcome of the task depends on the coordinated contribution of the two limbs and not on the simple replication of a trajectory. The robot can measure forces, velocities or coordination errors and modify the level of assistance depending on the subject's participation. Gerardin et al. used a bimanual robotic interface in which a common cursor was controlled by the coordinated action of the two limbs, allowing to quantify learning, speed–accuracy trade-off and coordination [11]. Similarly, the BiCAR system by Alves et al. integrates cooperative control, feedback and serious games in which performance depends on the contribution of both limbs [1].

Strategy	Signal/reference	Participation	Strengths	Main limitations
Passive / predefined	Programmed trajectory	Low	Repeatability; useful in severe impairment	Risk of reduced voluntary involvement [11, 18]
Mirror / master–slave	Movement of the less impaired limb	High on the master side	Personalized and intuitive reference	Symmetry does not represent all ADLs [7, 14, 17, 20]
Active-assisted / AAN	Tracking error + performance	Medium–high	Assistance proportional to need	Requires robust performance estimation [12]
EMG-triggered	Voluntary muscle activity	High	Assistance linked to motor intention	EMG variability and electrode setup [6]
Impedance / admittance	Position error or force/torque	Variable	Compliant and safe interaction	Parameter tuning and reliable sensors required [12, 15]
Cooperative / human-in-the-loop	Combined performance of both limbs	High	Directly trains coordination and task success	Greater control and complexity [1, 11]

Table 2.1: Summary of the main control strategies for robot-assisted upper-limb rehabilitation.

2.2. Sensor integration

Sensory integration represents the connection between the patient's movement and the behavior of the robotic system. Sensors can be used for three main functions: measuring kinematics, quantifying physical interaction and estimating motor intention. The choice of sensory modality directly influences the precision of the control, the ergonomics of the setup and the possibility of transferring the system from the laboratory to clinical or home contexts [9, 12].

Integrated encoders and kinematic sensors

Encoders are the most direct solution for measuring the joint configuration of the robot. In rigid systems they can provide high-precision position feedback and close the control loop at the joint. In Kwok and Yu's UULE, for example, absolute encoders and visual-inertial sensors are used on the master side to define the desired joint trajectory and on the slave side to measure the real feedback [14]. The main limitation is that the measurement directly describes the configuration of the robot, not necessarily the anatomical one of the subject; any misalignments between the robotic axis and the joint axis can introduce errors.

Force and torque sensors

Load cells, force/torque sensors and force sensing resistors allow the quantification of human-robot interaction and the contribution of the two limbs. In admittance control systems the force signal can be transformed into a speed command; in cooperative tasks it can instead be used to estimate the distribution of the contribution between the affected and non-affected side. The CAR/BiCAR system uses load cells to record the forces applied during the task, while the UULE integrates FSR sensors on the handles to recognize the grasp action in a virtual environment [1, 14].

Surface electromyography

Surface electromyography (sEMG) provides complementary information to kinematics, because it describes the level of muscle activation and can be used as a proxy for patient intention or commitment. It can directly trigger an intervention, as in EMG-triggered protocols [6], or be integrated with other modalities. In more recent systems, sEMG and kinematics are fused to adapt control to the residual capacity of the paretic limb; Chen et al., for example, combine sEMG of the affected limb and kinematics of the healthy side to dynamically modulate the mirroring ratio [7].

Inertial Measurement Units

Inertial Measurement Units (IMUs) are wearable sensors that typically integrate accelerometers, gyroscopes and, in some configurations, magnetometers. Through sensor fusion algorithms they allow the orientation of body segments to be estimated, as well as providing accelerations and angular velocities. Compared to optical systems, IMUs are compact, portable and less dependent on a structured measurement volume; these char-

acteristics make them particularly interesting for home rehabilitation and for monitoring functional tasks [9, 12].
The review by Cinnera et al., shows that IMUs have been used to evaluate joint mobility, muscle tone, voluntary movement control, and hand and arm use. The analysis reports a significant correlation between IMU-based kinematic variables and clinical assessments, supporting the integration between inertial sensing and conventional assessment [9]. This result is relevant because it shows that variables derived from IMUs can have clinical and not just technical significance.
For the use of IMUs in control, the critical step is the transformation from sensor orientation to anatomical kinematics. Bardi et al. proposed a real-time algorithm based on three IMUs positioned on the chest, arm and forearm, with extraction of five shoulder and elbow angles according to the ISB convention. The procedure uses N-pose and T-pose calibration and does not require the magnetometer [3].
The accuracy of IMUs, however, depends on the sensor-segment calibration, fixation stability and drift treatment. Little et al. also highlight that complex calibration procedures can limit clinical practicality, especially in patients with movement disorders [15]. It follows that the design of an IMU-based pipeline must consider not only numerical accuracy but also repeatability, simplicity of setup and robustness to repositioning.

Multimodal sensor fusion

In multimodal architectures, kinematic, bioelectrical, and interaction sensors are combined to obtain a more complete description of the patient's state. Fusion can increase the customization of control, but introduces more rigid requirements in terms of synchronization, update frequency, data management, and comfort. The review by Karasheva et al. highlights that multimodal integration is one of the most promising directions for sensor-driven systems, although it still remains mainly in the development or preclinical validation phase [12].

Sensor	Variable	Use in control	Advantages	Limitations
Encoder	Robot joint position/velocity	Position feedback	High precision at the robot level	Does not directly measure anatomical motion; misalignment [14]
Force/torque	Physical interaction	Admittance, cooperative control	Quantifies contribution and load	Requires a stable mechanical interface [1, 12]
sEMG	Muscle activation	Trigger, intention estimation, adaptation	Provides physiological information	Noise, fatigue, and electrode placement [6, 7]
IMU	Orientation, acceleration, angular velocity	Tracking, kinematic reference, assistance modulation	Wearable, wireless, and portable	Calibration, drift, and soft-tissue artefacts [3, 9, 15]
Multimodal	Kinematics + physiological signals + interaction	Adaptive closed-loop control	Greater personalization	Synchronization and system complexity [7, 12]

Table 2.2: Main sensing modalities used in robotic systems for upper-limb rehabilitation.

2.3. Coordination patterns

Bimanual coordination does not identify a single motor pattern. The two limbs can move simultaneously, alternately, with mirror-image trajectories, or with functionally different roles. The distinction between these patterns is essential, since the difficulty of the task, the level of interlimb coupling, and the neural circuits involved depend on the spatial and temporal relationship between the two limbs [11, 16].

Symmetric/in-phase pattern

In the in-phase symmetric pattern, the two upper limbs simultaneously perform analogous movements, characterized by a spatial and temporal correspondence between homologous segments. In rhythmic movements, this configuration generally involves the synchronous activation of corresponding muscle groups and represents one of the most stable bimanual coordination modalities. Typical examples include bilateral movements performed at the same time and according to a comparable motor pattern, such as rowing or some activities performed with both hands.
From a rehabilitation perspective, the in-phase pattern is particularly interesting because it simplifies the relationship between the two limbs and can favor the simultaneous involvement of the paretic and non-paretic sides. Indeed, the literature on bimanual coordination indicates that interlimb coupling tends to be more marked in in-phase conditions than in anti-phase configurations [16]. For this reason, synchronized bilateral movements have been frequently used in rehabilitation protocols and robotic systems dedicated to upper limb recovery [6, 18].

Symmetric/anti-phase pattern

In the anti-phase symmetric pattern, the two limbs perform spatially comparable movements, but according to an opposite or alternating temporal relationship. In other words, while one limb performs a given phase of the movement, the other performs the complementary phase. Representative examples are pedaling or alternating sequences of flexion and extension of the upper limbs.
Compared to the in-phase configuration, the anti-phase pattern generally requires more complex temporal control and presents less spontaneous coordination stability. The assessment of this type of coordination can therefore provide information on the subject's ability to maintain a controlled temporal relationship between the two sides.

Asymmetric/complementary pattern

In the asymmetric or complementary pattern, the two limbs participate in the same functional task while performing different but coordinated roles. The trajectories, amplitudes of movement and actions required on the two sides can therefore be different, as long as they contribute to achieving a common goal. A typical example is represented by activities in which one hand stabilizes an object while the other performs a manipulation action.
This configuration is of particular importance from a rehabilitation point of view, since

numerous activities of daily living (ADL) require asymmetric cooperation between the upper limbs. Gerardin et al. explicitly distinguish symmetric and asymmetric bimanual tasks, underlining how many complex functional activities belong to the second category [11]. Similarly, cooperative robotic systems can be designed so that the success of the task depends on the coordinated, but not necessarily identical, contribution of the two limbs [1].

Mirror-symmetric pattern

The mirror-symmetric pattern represents a particular bilateral configuration in which the movement performed by the master limb is transformed into a geometrically corresponding movement of the contralateral limb. In the context of post-stroke rehabilitation, the non-paretic side can therefore be used as the source of the kinematic reference, while the robotic system reproduces or assists the corresponding movement on the affected side. This paradigm is closely associated with master–slave architecture. Unlike a pre-programmed trajectory, the reference derives directly from the voluntary movement produced by the subject and can therefore adapt to the individual characteristics of the execution.
Strategies of this type have been implemented both in distal exoskeletons for the hand and in bilateral devices for more proximal segments [14, 17, 20].
More recent approaches also introduce adaptive mirroring strategies, in which the correspondence between the master side and the assisted side can be modulated according to the patient's residual capabilities [7].
For the paradigm considered in this thesis, the mirror-symmetric pattern takes on particular relevance, since it allows the kinematics acquired by the unaffected limb to be used as a reference for the generation of the assisted contralateral movement.

Pattern	Relationship between limbs	Example	Rehabilitation relevance
Symmetric / in-phase	Similar movements performed simultaneously by both limbs	Synchronous bilateral movement like rowing or drumming	Stable coordination pattern characterized by strong interlimb coupling [6, 16]
Symmetric / anti-phase	Similar movements performed with an alternating or opposite temporal relationship	Alternating flexion–extension like cycling	Requires greater control of the temporal relationship between the two limbs [16]
Asymmetric / complementary	Different but coordinated roles or trajectories directed toward a common goal	Stabilizing with one hand while manipulating with the other	High relevance to ADLs, but greater control complexity [1, 11]
Mirror-symmetric	The master-side movement is transformed into the corresponding contralateral movement	Master–slave modality	Suitable for rehabilitation strategies in which the non-paretic limb provides the reference for the assisted limb [7, 14, 17, 20]

Table 2.3: Main coordination patterns relevant to bimanual rehabilitation.

2.4. Use case and exercise

Task selection is a fundamental element of the rehabilitation protocol. A technically accurate system used only for isolated movements can produce kinematic improvements that are difficult to transfer to daily activities. For this reason, the most recent literature tends to integrate reaching, grasping, object manipulation, ADL activities, and serious games within task-oriented protocols [1, 2, 4, 8, 11].

Reaching and grasping

Reaching and grasping tasks are widely used because they involve the coordination of shoulder, elbow and distal segments and allow to extract interpretable kinematic param-

eters, such as duration, velocity, smoothness, path length and range of motion. Christopher and Johnson employed a task-oriented robot-assisted training consisting of reaching, grasping, self-care and 2D/3D movement modules, highlighting the value of temporal and spatial metrics to describe the control of the paretic side [8].

Activity of daily living

ADL exercises enhance the validity of training, as they require motor sequences with an immediately recognizable functional goal. Wearable upper limb robots have been proposed for activities such as drinking, eating, reaching, and personal hygiene [2]. In bimanual systems, the additional challenge lies in reproducing cooperation between the hands and ensuring that the robotic assistance does not completely replace the subject's strategy. Kwok and Yu used a symmetric bimanual task of transferring a virtual object to the mouth. The subject approached the object with their hands, grasped it and completed the transfer while the exoskeleton operated in transparent mode or with master–slave assistance [14]. The task represents an example of how an ADL task can be directly integrated into the control framework combining kinematics, grasp detection, and visual feedback, as shown in Figure 2.1.

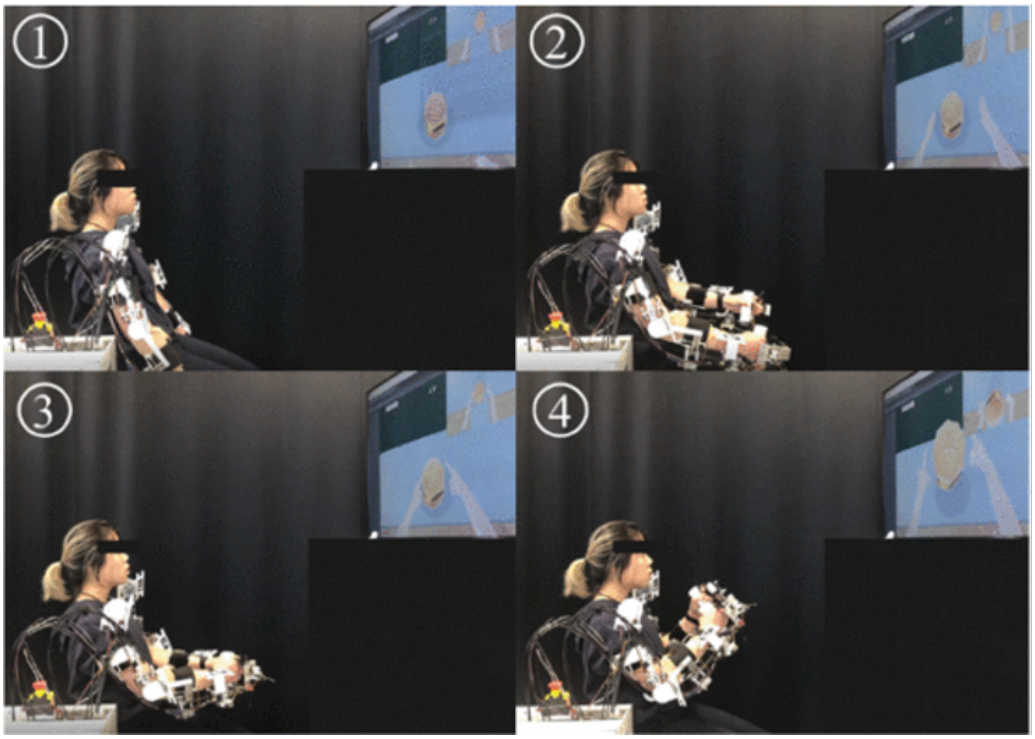

Figure 2.1: Experimental sequence of the symmetric bimanual task performed with the UULE: starting position, approaching the object, grasping, and transferring it toward the mouth [14].

Serious game and feedback

Serious games are used to increase engagement and tolerability of repetition, while maintaining the ability to record quantitative variables. Alves et al. developed the CAR/BiCAR system associated with several games, including Rehab Basketball, Square Apple, Grabbing Apple, Paper Plane, Motorcycle, MineCart, and Sakura Flowers (Figure 2.2). The system records duration, movement, and forces and can adapt assistance based on the user's participation [1].

The contribution of serious games is not limited to motivation: the virtual task can impose timing, accuracy, and cooperation constraints that make bimanual performance measurable. However, the choice of game must remain consistent with the clinical objective and not replace the need to verify transfer to real-world activities.

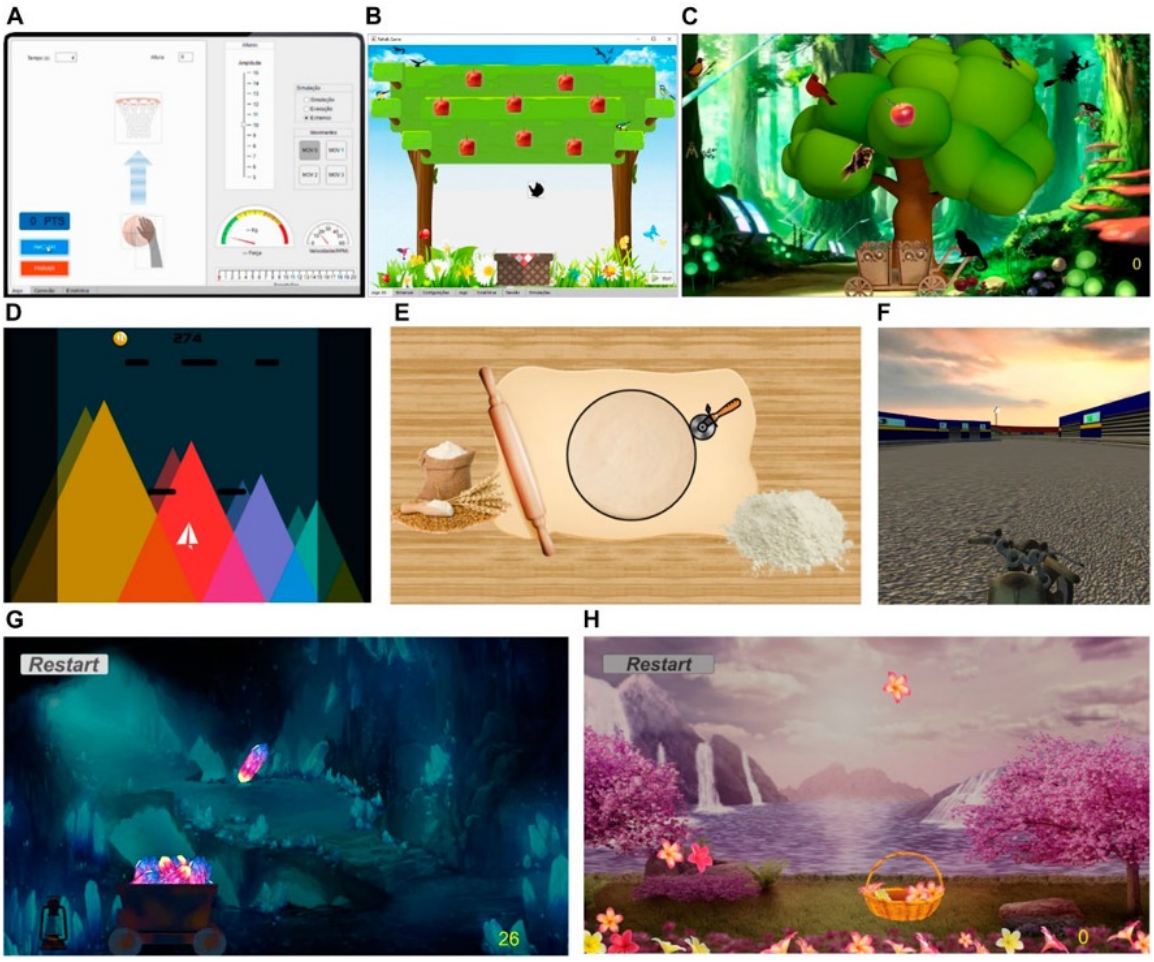

Figure 2.2: Examples of serious game interfaces developed for the CAR/BiCAR systems: Rehab Basketball, Square Apple, Grabbing Apple, Paper Plane, Round Pizza, Motorcycle, MineCart, and Sakura Flowers [1].

Drinking task

Among ADL activities, the drinking task represents a particularly interesting use case because it combines reaching, grasping, transporting the object to the mouth, and returning to the starting position. Christopher and Johnson broke the task down into four events: reaching and grasping the cup, lifting it to the mouth, returning and releasing it, and returning to the resting position. Their analysis showed that control of the paretic side during a bilateral task is affected by the presence and movement of the non-paretic limb, suggesting a role for interlimb coupling in performance transfer [8].
For the paradigm developed in this thesis, the drinking task presents three methodological advantages: it is functionally meaningful, can be easily segmented into kinematic subphases, and is compatible with a reference generated by the unaffected side. At the same time, the task highlights a limitation of simple mirroring: in real ADLs, the two limbs may have different roles. Mirror-symmetric therefore represents a controllable and repeatable initial strategy, not necessarily the definitive model for every bimanual activity.

2.5. Literature gap

Four main critical issues emerge from the literature reviewed, which motivate the present study. The first concerns the transfer from motor ability to function. Boardsworth et al.'s analysis, identifies a small positive effect of robotics on upper limb capacity, but does not highlight a significant overall advantage in ADLs compared to conventional equivalent rehabilitation. Outcomes are also influenced by device and program characteristics, including assistance, mobilized joints and degrees of freedom [4]. Consequently, efficacy cannot be generically attributed to the presence of the robot, but depends on how the system is used.

The second critical issue concerns bimanual rehabilitation. Although numerous devices have been developed, clinical evidence remains heterogeneous. Sheng et al. note that only a portion of the included studies demonstrated a superiority of bilateral training over unilateral training and emphasize the need for equivalent protocols and more uniform evaluation criteria [18]. In parallel, Liu et al. show that many studies claim to study bimanual coordination without directly measuring interlimbic organization using appropriate kinematic indices [16].

The third critical issue concerns the role of IMUs. Inertial sensing is now well-established as a tool for assessing and monitoring the upper limb, with evidence of correlation with clinical scales [9]. There are also examples of IMUs integrated into the control of exosuits

or exoskeletons [15, 20]. However, the sensor-driven review by Karasheva et al. indicates that a significant portion of multimodal and adaptive architectures remains at the development or validation stage on healthy subjects, with limited clinical translation [12].

The fourth, more specific, critical issue emerges when comparing available mirror systems. In the analyzed corpus, control of the paretic limb via the unaffected side has been implemented primarily in distal hand devices [17, 20], in bilateral exoskeletons using robot-integrated sensing [14], or in more complex multimodal systems [7]. However, an architecture in which a small set of wearable IMUs, independent of the robot and positioned on the trunk and unaffected limb, reconstructs proximal kinematics in real time and generates a mirror reference for controlling a unilateral exoskeleton, is underrepresented.

This configuration has potential advantages: it separates the acquisition module from the assistive device, allows for verification and validation of the kinematics before integration with the actuators, and maintains a movement actually produced by the patient as a reference. At the same time, it introduces methodological issues that must be explicitly addressed, including quaternion conventions, sensor-segment calibration, body frame definition, left-right transformation, cross-talk between degrees of freedom, and reconstruction repeatability.

2.6. Aim of the study

Given the state of the art and the identified gaps, the overall objective of this thesis is to define a bimanual-assisted rehabilitation paradigm in which the movement of the unaffected limb can serve as the kinematic reference for robotic assistance of the contralateral limb, according to a mirror/master-slave logic.

In the experimental setting addressed in this work, the primary objective is to develop and validate the IMU-based kinematic module required for this paradigm. Specifically, the work aims to: acquire the orientation of the chest, arm, and forearm in real time using three NGIMU sensors; define calibration conventions and procedures consistent with upper limb kinematics; reconstruct a three-dimensional representation of the movement and joint variables useful for validation; implement a robust mirror transformation with respect to the master side; and quantify the quality of the reconstruction using an experimental protocol based on range of motion, cross-talk, hand trajectory, velocity, duration, distance from the sagittal plane, residual angular variation, and acquisition quality.

Integration with the exoskeleton constitutes the application level toward which the architecture is oriented: the validated pipeline must provide a kinematic reference that is

sufficiently consistent, repeatable, and interpretable to be converted into joint or trajectory commands for the assisted side. From this perspective, the drinking task represents the reference functional use case, as it allows mirror control to be linked to a meaningful daily activity and maintains continuity with the rehabilitation goals.

The thesis therefore does not intend to demonstrate, at this stage, the clinical efficacy of a comprehensive post-stroke treatment; rather, it aims to validate the technological and kinematic prerequisites necessary to implement a future bimanual robot-assisted protocol based on the physiological movement of the unaffected side.

3 | Materials and methods

This chapter describes the materials and methods used to acquire, process, and visualize upper-limb kinematics in real time using three inertial sensors. In this thesis, the term *simulation* refers to the three-dimensional reconstruction driven by the orientations measured by the NGIMU units, rather than to the generation of synthetic motion. The system represents the motion-reconstruction component of a master–slave paradigm in which the unaffected upper limb can provide a kinematic reference for the contralateral limb.

The processing pipeline was organised into separate modules for data acquisition, temporal synchronisation, sensor-to-segment calibration, kinematic reconstruction, visualisation, recording, and offline analysis. This modular structure made it possible to trace each transformation from the raw quaternion data to the final outcome measures.

The experimental procedure was designed to evaluate repeatability, internal kinematic consistency, sensitivity to sensor repositioning, and agreement with an external video-based human-pose estimation system.

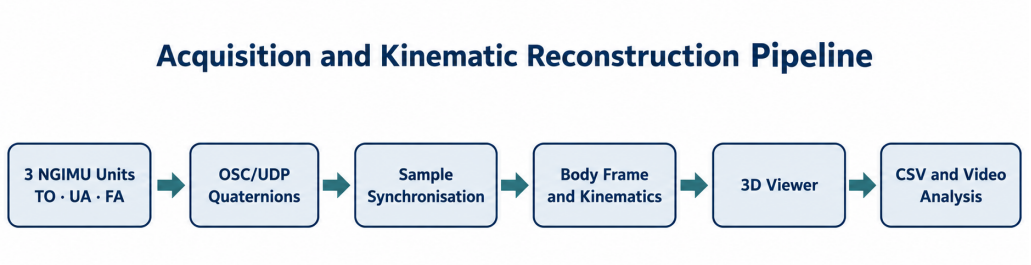

Figure 3.1: Modular architecture of the processing pipeline, including NGIMU acquisition, synchronization, kinematic processing, visualization, recording, and analysis.

3.1. Materials

NGIMU sensors and hardware configuration

The acquisition system consisted of three NGIMU units (Next Generation Inertial Measurement Unit, x-io Technologies Ltd., Bristol, United Kingdom), positioned on the trunk, upper arm, and forearm of the master side. In the software, the sensors were identified as TO (torso), UA (upper arm), and FA (forearm). The trunk sensor was used to define a body-fixed reference frame, allowing upper-limb motion to be expressed relative to the participant's trunk rather than to the room.

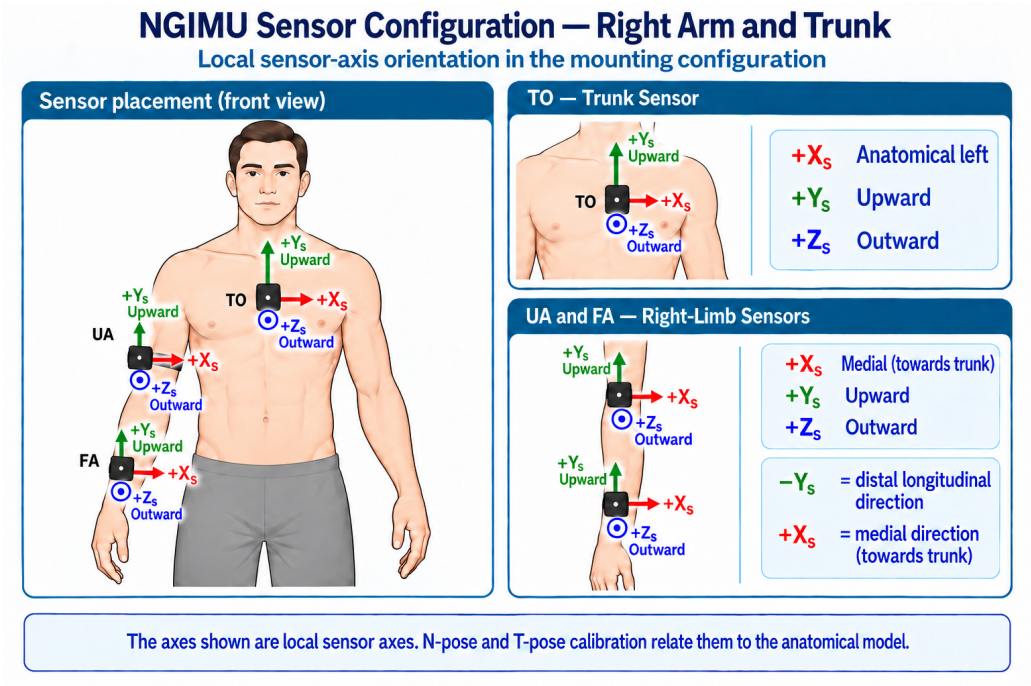

Figure 3.2: Schematic positioning of the three NGIMU units on the master side. (Generated with AI)

Whenever the master side was changed, the UA and FA sensors were moved to the opposite limb and the complete sensor-to-segment calibration was repeated. Sensor placement was documented using anatomical landmarks and sensor orientation (strictly oriented with $+X$ pointing to the left and $+Y$ pointing up).

The OSC message `/quaternion` was transmitted over Wi-Fi using UDP at a nominal frequency of 50 Hz. In the present configuration, ports 8100, 8103, and 8104 were assigned to TO, UA, and FA, respectively. Quaternion components were received in the order specified at program start and converted internally to the order $[w, x, y, z]$.

Quaternions and internal convention

The orientation of each sensor was represented by a unit quaternion

$$\mathbf{q} = \begin{bmatrix} w & x & y & z \end{bmatrix}. \tag{3.1}$$

Every received quaternion was reordered, normalised, and sign-aligned with the preceding sample. The sign-alignment step selected either $\mathbf{q}$ or $-\mathbf{q}$ according to temporal continuity; these two quaternions represent the same physical rotation.

The rotation of a local vector $\mathbf{v}$ was calculated as

$$\mathbf{v}' = \mathbf{q} \begin{bmatrix} 0 & \mathbf{v}^{\mathrm{T}} \end{bmatrix}^{\mathrm{T}} \mathbf{q}^{*}, \tag{3.2}$$

where $\mathbf{q}^{*}$ is the quaternion conjugate. Quaternion multiplication was applied without normalising the pure-vector quaternion, so that the magnitude of the rotated vector was preserved. When required by the NGIMU output convention, the received orientation quaternion was inverted before its use in the kinematic model. The same convention was applied to TO, UA, and FA throughout a recording session.

Anthropometric parameters

The anthropometric dimensions of the participants were manually measured before data acquisition. The length of the Upper-arm was measured from the acromial region to the center of the elbow joint, the length of the forearm from the center of the elbow joint to the center of the wrist joint, the width of the shoulder as the distance between the right and left acromial landmarks, and the height of the seated shoulder from the floor to the acromial level. All measurements were entered in centimetres and converted to metres by the software.

These values were used to reconstruct the shoulder, elbow, and wrist positions and stored with the participant and calibration data.

3.2. Methods: NGIMU simulation

The processing workflow consisted of the following steps: reception of the three sensor quaternions, temporal synchronisation, sensor-to-segment calibration, construction of the trunk-fixed reference frame, transformation of the segment directions into that frame,

calculation of shoulder and elbow variables, rigid-chain reconstruction, visualisation, and data recording.

3.2.1. Conventions used and modifications

Evolution from the original pipeline

The original upper-limb tracking framework supported a larger sensor configuration and used rotation matrices as its main orientation representation. For the master–slave application considered here, the system was reduced to three NGIMU units and converted to a quaternion-based implementation. One real upper limb was reconstructed at a time, while the contralateral limb was generated as a virtual representation.

The revised pipeline introduced a trunk-fixed reference frame, independent calibration of the UA and FA longitudinal axes, consistent RIGHT and LEFT side management, participant-specific anthropometry, and temporal synchronisation.

Body-fixed reference frame

The body frame was rigidly attached to the trunk and defined as follows:

- $+X$: towards the participant's right side;
- $+Y$: anteriorly;
- $+Z$: superiorly.

For the TO sensor, the local directions $+X$, $+Z$, and $+Y$ corresponded approximately to the anatomical leftward, forward, and upward directions. These configured axes were rotated into the world frame by the TO quaternion and orthonormalised. Let $\mathbf{R}_{WB}$ be the matrix whose columns are the rightward, forward, and upward body axes expressed in the world frame. A vector expressed in world coordinates was transformed into the body frame as

$$\mathbf{v}_B = \mathbf{R}_{WB}^{\mathrm{T}} \mathbf{v}_W. \tag{3.3}$$

This transformation removed the effect of a common rotation of the participant and allowed limb motion to be interpreted relative to the trunk.

Sensor-to-segment calibration: N-pose

The N-pose was used to estimate separately the longitudinal anatomical direction of the upper arm in the UA sensor frame and the longitudinal direction of the forearm in the FA sensor frame. The participant sat upright with the arm alongside the body and the elbow extended. In this pose, both segment directions were assumed to coincide with the downward body direction

$$\mathbf{e}_{\text{down},B} = \begin{bmatrix} 0 & 0 & -1 \end{bmatrix}^{\mathrm{T}}. \tag{3.4}$$

The downward direction was first expressed in world coordinates and then transformed into the local frame of each sensor. If $\mathbf{R}_{WU,N}$ and $\mathbf{R}_{WF,N}$ denote the UA and FA orientations during the N-pose, the calibrated local longitudinal axes were

$$\mathbf{a}_U = \mathbf{R}_{WU,N}^{\mathrm{T}} \mathbf{R}_{WB,N} \mathbf{e}_{\text{down},B}, \tag{3.5}$$

$$\mathbf{a}_F = \mathbf{R}_{WF,N}^{\mathrm{T}} \mathbf{R}_{WB,N} \mathbf{e}_{\text{down},B}. \tag{3.6}$$

This separate calibration is essential because the two sensors can have different mounting orientations. It allows the anatomical segment direction to be reconstructed without assuming that the local axes of UA and FA are mutually aligned.

Functional calibration: T-pose and F-pose

After the N-pose, the participant elevated the master arm laterally with the elbow extended. The projected humeral direction measured in this pose defined the positive lateral elevation direction. The raw elevation measured in the T-pose was stored as the functional reference that was mapped to an AoE of exactly 90°.

An additional forward pose, F-pose, was then acquired with the arm extended anteriorly at approximately shoulder height. Its horizontal projection defined PoE = 0°. The T-pose defined PoE = +90° on both the RIGHT and LEFT master sides.

The final shoulder basis contained a forward unit vector $\mathbf{e}_{\text{fwd}}$, a lateral unit vector $\mathbf{e}_{\text{lat}}$, and the downward vector $\mathbf{e}_{\text{down}}$. Changing the master side or repeating the N-pose invalidated the previous functional calibration; the N-, T-, and F-poses were therefore always performed in sequence.

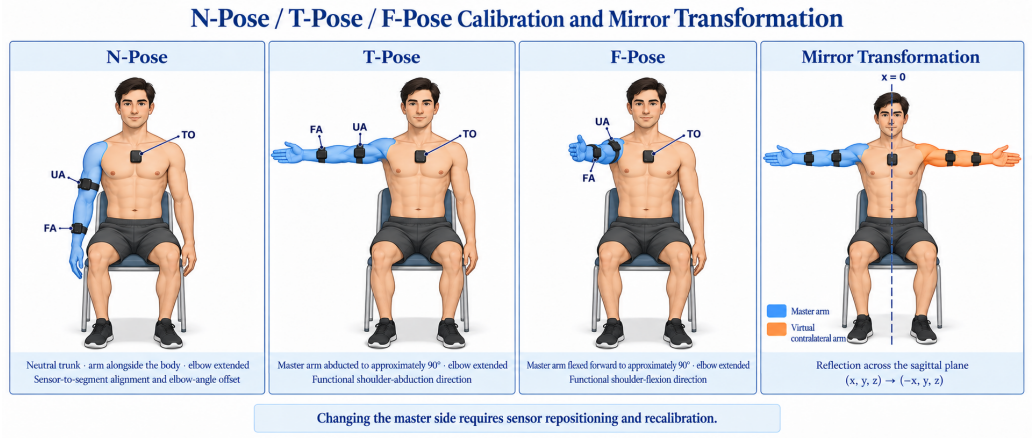

Figure 3.3: N-pose, T-pose and F-pose calibration procedures and mirror transformation across the sagittal plane.(Generated with AI)

Definition of shoulder variables

The shoulder variables describe humero-thoracic motion because scapular motion was not measured independently. Humeral axial rotation was not estimated, since the longitudinal direction of the humerus alone does not identify rotation around that same axis.

For each synchronised sample, the calibrated upper-arm direction was reconstructed in the world frame and then expressed in the body frame:

$$\mathbf{u}_B = \mathbf{R}_{WB}^{\mathrm{T}} \mathbf{R}_{WU} \mathbf{a}_U. \tag{3.7}$$

After normalisation, its components in the calibrated shoulder basis were

$$c_{\mathrm{fwd}} = \mathbf{u}_B \cdot \mathbf{e}_{\mathrm{fwd}}, \tag{3.8}$$

$$c_{\mathrm{lat}} = \mathbf{u}_B \cdot \mathbf{e}_{\mathrm{lat}}, \tag{3.9}$$

$$c_{\mathrm{down}} = \mathbf{u}_B \cdot \mathbf{e}_{\mathrm{down}}. \tag{3.10}$$

The Angle of Elevation was calculated using the arctangent:

$$\theta_{\mathrm{AoE,raw}} = atan2\left(\sqrt{c_{\mathrm{fwd}}^2 + c_{\mathrm{lat}}^2}, c_{\mathrm{down}}\right). \tag{3.11}$$

This formulation provides a continuous range from 0° for the arm directed downward to 180° for the arm directed upward beyond the head and is not restricted to the principal range of the inverse sine function.

Let θ_T be the raw elevation measured during the T-pose. The calibrated AoE was obtained through the continuous mapping

$$\theta_{\text{AoE}} = \begin{cases} 90^\circ \dfrac{\theta_{\text{AoE,raw}}}{\theta_T}, & \theta_{\text{AoE,raw}} \leq \theta_T, \\ 90^\circ + 90^\circ \dfrac{\theta_{\text{AoE,raw}} - \theta_T}{180^\circ - \theta_T}, & \theta_{\text{AoE,raw}} > \theta_T. \end{cases} \tag{3.12}$$

Consequently, the N-pose corresponds to approximately 0° and the individual T-pose reference corresponds exactly to 90°.

The raw Plane of Elevation was calculated as

$$\theta_{\text{PoE,raw}} = atan2(c_{\text{lat}}, c_{\text{fwd}}). \tag{3.13}$$

The F-pose was assigned PoE = 0° and the T-pose PoE = +90°. The measured F-to-T separation was used to scale the sector between the two poses. Positive PoE therefore indicated elevation from the anterior direction towards the calibrated lateral direction, independently of whether the right or left arm was the master.

When the arm approaches the downward or upward vertical direction, its projection onto the transverse plane approaches zero. In this condition, PoE is mathematically undefined and highly sensitive to noise. PoE was therefore reported only when the calibrated AoE was between 15° and 165°; outside this range it was stored as an undefined value and excluded from numerical PoE analyses.

Elbow flexion-extension

The calibrated forearm direction was reconstructed independently from the FA quaternion:

$$\mathbf{f}_B = \mathbf{R}_{WB}^{\mathrm{T}} \mathbf{R}_{WF} \mathbf{a}_F. \tag{3.14}$$

After normalising $\mathbf{u}_B$ and $\mathbf{f}_B$, the unsigned geometric flexion angle was calculated as

$$\theta_{E,\text{raw}} = atan2\left(\left\|\mathbf{u}_B \times \mathbf{f}_B\right\|, \mathbf{u}_B \cdot \mathbf{f}_B\right). \tag{3.15}$$

This formulation returns approximately 0° when the two segments are aligned and increases with elbow flexion. It is invariant to a common rotation of both segments and

does not require the local UA and FA sensor axes to be aligned. If a small residual angle $\theta_{E,N}$ remained in the N-pose, the reported flexion value was

$$\theta_E = \max\left(0, \theta_{E,\text{raw}} - \theta_{E,N}\right). \tag{3.16}$$

The present three-sensor model reports the magnitude of elbow flexion-extension. It does not estimate forearm pronation-supination.

Acquisition, synchronisation, and time base

Data from the three sensors were received independently of the graphical display. At each quaternion was assigned a timestamp when it arrived at the computer, using a common monotonic clock. These timestamps were used to align the data in time, although they did not guarantee simultaneous measurements by the sensors.

The trunk sensor (TO) provided the reference timestamps. At each reference instant, upper-arm (UA) and forearm (FA) orientations were estimated using spherical linear interpolation (SLERP) between the samples immediately before and after that instant. For each sensor, the two samples had to be no more than 60 ms apart, and the nearest sample had to be within 30 ms of the reference instant. Samples failing these checks were discarded and counted.

Each accepted sample was recorded once. The viewer refreshed at 60 frames per second, while the recording rate depended on the number of accepted samples.

3.2.2. 3D simulation

The three-dimensional simulation represented the trunk and upper limb as a rigid kinematic chain. The upper-arm and forearm directions were expressed in the body frame and combined with the participant-specific segment lengths.

Let $s = +1$ for the RIGHT side and $s = -1$ for the LEFT side. The shoulder point was defined as

$$\mathbf{p}_S = \begin{bmatrix} s\,W_S/2 & 0 & H_S \end{bmatrix}^{\mathrm{T}}, \tag{3.17}$$

where W_S is shoulder width and H_S is seated shoulder height. Elbow and wrist positions were then reconstructed as

$$\mathbf{p}_E = \mathbf{p}_S + L_{UA}\mathbf{u}_B, \tag{3.18}$$

$$\mathbf{p}_W = \mathbf{p}_E + L_{FA}\mathbf{f}_B. \tag{3.19}$$

The reconstructed wrist coordinate was therefore a model-based estimate derived from sensor orientation, calibration, and manual anthropometry. It was not a directly measured hand or wrist position.

Three-dimensional viewer

The Pygame viewer displayed the trunk, the measured master limb, the virtual slave limb, and the body-fixed axes. Sensor axes and the calibrated shoulder basis could be shown. The viewer used the output of the kinematic model and did not perform an independent second angle calculation.

The displayed segment lengths were the same participant-specific lengths used in the recorded rigid-chain reconstruction. Camera viewpoint changes affected only the visual presentation and did not modify the body frame, joint angles, or stored coordinates.

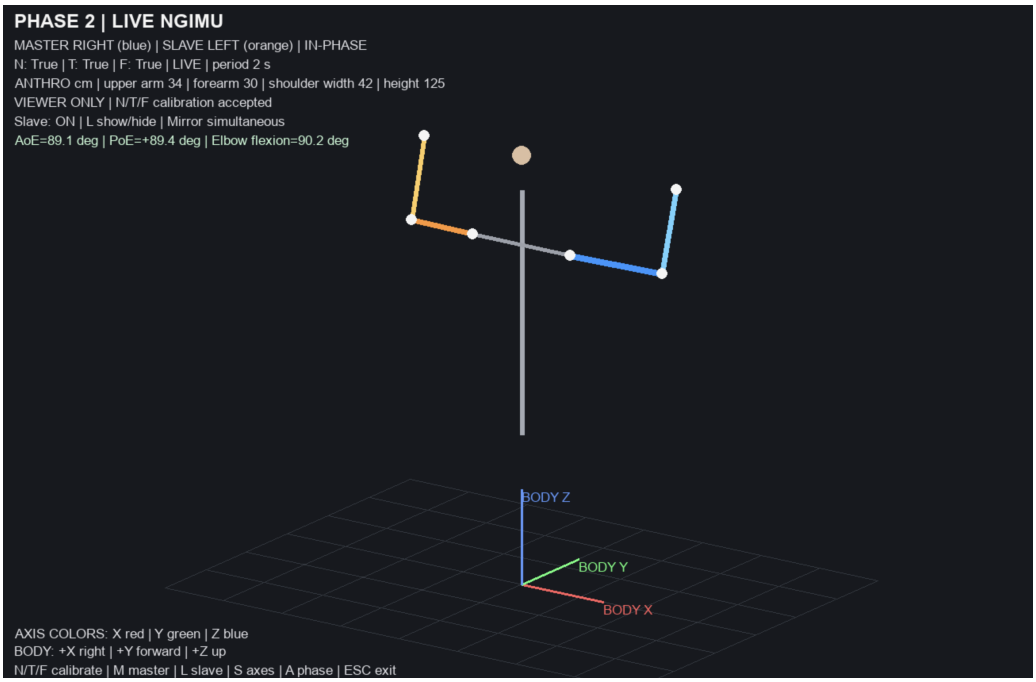

Figure 3.4: 3D viewer.

Mirror representation

In simultaneous mirror mode, the slave limb was generated by reflecting the reconstructed master points across the trunk sagittal plane $x = 0$:

$$(x, y, z) \longrightarrow (-x, y, z). \tag{3.20}$$

The software also supported an anti-phase mode. In this mode, the master quaternions from one half of the specified cycle period earlier were reconstructed and then spatially mirrored. Quaternion interpolation was used to obtain the delayed orientation. This mode assumes an approximately periodic movement with a known and sufficiently constant cycle duration and was not used as the primary condition in the main validation protocol.

In both modes, the slave limb was a virtual kinematic reference. It did not represent a measured second arm and did not correspond to motion physically imposed by an exoskeleton.

Data recording

The recorder saved one CSV row for each accepted sample. Recorded variables included relative time, sample index, AoE, PoE, elbow flexion, reconstructed wrist coordinates, and the input TO, UA, and FA quaternions in the $wxyz$ convention.

3.3. Testing protocol

Technical validation of an upper limb kinematic system and mirrored bimanual simulation based on three inertial measurement units

Objective

Inertial measurement units (IMUs) allow the joint kinematics of the upper limb to be estimated using segment orientations and kinematic models. The quality of the estimation depends on the definition of the reference systems and the sensor-segment calibration.

The primary objective of the study is to evaluate the repeatability and internal coherence of the kinematic reconstruction of the upper limb obtained from three IMUs positioned on the trunk, upper arm and forearm, and its use in a mirrored bimanual simulation. The specific objectives are:

• quantify the repeatability of the range of motion (ROM) in isolated shoulder and elbow

movements;

• quantify the kinematic cross-talk of non-target degrees of freedom during mono-planar movements;

• evaluate the repeatability of the reconstructed three-dimensional trajectory of the wrist during a multi-joint functional task;

• quantify the variability introduced by the removal and repositioning of sensors;

• compare held joint angles and lateral wrist position with OpenCap pose estimation and check the simultaneous mirrored movement of the virtual arm.

Participant and experimental design

Ten healthy adults (aged $\geq$ 18 years) will be recruited. This sample is used for a preliminary evaluation of the system's performance and repeatability, without the aim of providing a definitive estimate of clinical accuracy or reliability.

Inclusion criteria: ability to independently perform the required tasks and absence of pain or significant functional limitations at the time of testing.

Exclusion criteria: known neurological pathologies or musculoskeletal conditions of the upper limb/trunk that could alter the execution of the experimental movements.

Kinematic model

The model calculates the shoulder elevation angle and the plane of elevation. The elevation angle describes how much the upper arm is raised relative to the downward direction of the trunk. An elevation of approximately 0° corresponds to the arm resting along the body, while increasing values indicate raising of the arm, independently of whether this occurs anteriorly, laterally, or in an intermediate direction.

The plane of elevation describes the direction around the trunk in which the arm is raised. It distinguishes, for example, an arm elevated mainly in the sagittal plane from one elevated mainly in the frontal plane or in an intermediate plane such as the scapular plane. Together, elevation and plane of elevation provide a compact description of upper-arm direction: the elevation angle describes how much the arm is raised, whereas the plane of elevation describes in which direction the elevation occurs.

Shoulder internal/external rotation is not estimated by the current model because the reconstruction is based primarily on the longitudinal direction of the upper arm and does not independently determine rotation around this axis.

Elbow flexion is obtained from the relative orientation of the upper-arm and forearm longitudinal directions. More specifically, the angle between the two segment directions is calculated and corrected using the reference value acquired during the N-pose, so that the reconstructed elbow angle represents flexion relative to the calibrated neutral configuration.

A rigid-segment kinematic model is subsequently used to reconstruct the spatial position of the elbow and wrist. Starting from the shoulder position, the elbow is obtained by projecting the calibrated upper-arm direction according to the participant-specific upper-arm length. The wrist is then reconstructed from the elbow position using the forearm direction and forearm length. Therefore, wrist position is not directly measured by an additional sensor but is estimated from segment orientations and anthropometric measurements.

Anthropometric parameters: before acquisition, the length of the arm, the length of the forearm and the shoulder width will be provided for each participant with anthropometric parameters estimated directly on the subject with a meter. These values will be used in the reconstruction of the elbow and wrist position for the B1 and A2 spatial analyses.

For the external validation procedures, two smartphones mounted on fixed supports and OpenCap pose estimation are used as independent visual references.

Sensor-segment calibration and change of the master side

Sensor-to-segment calibration is performed separately for each side. The participant sits on a stable chair without armrests and the trunk upright, consistent with the intended seated upper limb rehabilitation application. A backrest or wall behind the chair provides a postural reference to limit compensatory movements without obstructing the arm. All tasks are performed seated.

1. N-pose: participant seated, trunk neutral, arm at the side and elbow extended. The pose defines the anatomical DOWN direction of the arm, calibrates the longitudinal axes of UA and FA, and defines elbow zero.

2. T-pose: after the N-pose, the master arm is brought laterally to approximately 90° of elevation with the elbow extended. The T-pose defines the functional 90° angle of elevation (AoE).

3. F-pose: after the T-pose, the master arm is brought frontal to reach the centre of the trunk with the elbow extended. This final pose defines the 0° plane of elevation (PoE).

When the master side is changed, the previous calibration is not maintained: it is therefore

necessary to re-run the N-pose, T-pose and F-pose. The comparison between the right and left sides serves to verify that the system maintains the same anatomical interpretation of movements and a consistent sign convention. However, the ROM values of the two limbs do not need to be equal, as there may be normal physiological differences between the right and left sides.

Main experimental protocol

Each recorded trial contains a single complete execution of the movement. The movements are performed at a comfortable and controlled speed. Five repetitions are recorded per task and per side. An initial stationary period of approximately 2 s will provide the baseline. In A1, the participant will move towards a target at approximately 90°, hold the reached position and return. The target guides execution, the actual reached angle, will be measured and compare with the one evaluated from OpenCap pose estimation.

	Task	**Execution**	**Outcome**
A1.1	Shoulder flexion/extension	N-pose → about 90° anterior flexion → hold for approximately 3 s for a photograph → come back in N-pose; elbow kept extended and trunk still.	ROM flexion; Cross-talk abduction and elbow; Video angle comparison.
A1.2	Shoulder abduction/adduction	N-pose → about 90° lateral abduction → hold for approximately 3 s for a photograph → come back in N-pose; elbow kept extended and trunk still.	ROM abduction; Cross-talk flexion and elbow; Video angle comparison.
A1.3	Elbow flexion/extension	Elbow flexion to approximately 90° → hold for approximately 3 s for a photograph → return to extension; arm held at side and trunk still.	ROM elbow; Cross-talk shoulder; Photographic angle comparison.
A2	Hand-to-mouth	From N-pose, lightly touch the centre of the lips with the same finger, then return. Keep head and trunk still; check successful contact.	Reconstructed wrist trajectory repeatability; Dispersion at the turning point.

	Task	Execution	Outcome
B1	Midline reach	Reach three anatomical targets on the body centreline, then return.	Coordinates of the wrist during the touching phase; Comparison of lateral and vertical wrist position with the geometrical reference.

Table 3.1: Principal evaluation task.

The main protocol includes 4 tasks × 5 repetitions × 2 sides = 40 recorded trials for A1 and A2 and 1 task x 3 repetitions x 2 sides = 6 repetitions for B1 per participant with a total of 46 recorded trials. Rest periods of at least 30 s are required between task blocks and a rest period of at least 2 min between the two sides. The mirrored bimanual simulation will run during the same trials, without additional acquisition blocks. The master arm will reproduce the measured movement, while the contralateral virtual slave will move simultaneously as its reflection across the sagittal plane. Both right and left master conditions will be tested. Correct side assignment, visible continuity and mirrored motion will be checked, and any anomalies will be recorded. This is a qualitative functional check; the system does not measure the movement of a second real arm.

Trial validity criteria

A trial is considered valid when:

• N-pose/T-pose/F-pose calibration of the current side is complete and accepted;

• TO, UA and FA data are present for the entire analysed window;

• there are no discontinuities or packet losses that will compromise the reconstruction;

• the task follows the defined procedure; video of the participant support the external reference and execution checks, while the viewer video documents the simulation;

• the task is performed according to the defined procedure, which can also be verified via the viewer video;

• there are no evident sensor shifts or voluntary interruptions during the trial. Invalid trials are excluded from the analysis and repeated.

Outcome definition

Isolated movements A1

For each isolated movement, the main joint angle involved in the task will be analysed. Shoulder flexion/extension will be considered for A1.1, shoulder abduction/adduction for A1.2, and elbow flexion/extension for A1.3.

The range of motion (ROM) will be calculated as the difference between the maximum and minimum values of the target angle recorded during each trial:

$$ROM = \theta_{\max} - \theta_{\min} \tag{3.21}$$

To evaluate whether the model correctly separates the different joint movements, cross-talk will also be calculated for the non-target angles. Cross-talk will be defined as the maximum absolute variation of the non-target angle from its initial reference value:

$$CT = \max_t |\theta_{\text{non-target}}(t) - \theta_{\text{baseline}}| \tag{3.22}$$

The baseline will be calculated from the initial stationary phase of the trial, during which the participant maintains the starting N-pose.

The movements will also be recorded using two smartphones mounted on fixed supports and analysed with OpenCap tracking system. The shoulder and elbow angles derived from the video-based analysis will be used as an external reference for comparison with the corresponding IMU-derived angles.

Before comparison, the two signals will be temporally aligned and expressed using compatible angle definitions and sign conventions.

The comparison will include the difference in ROM between the two systems:

$$\Delta ROM = ROM_{\text{IMU}} - ROM_{\text{AI}} \tag{3.23}$$

The agreement between the complete angular trajectories will also be evaluated using the root mean square error (RMSE):

$$RMSE_\theta = \sqrt{\frac{1}{N}\sum_{i=1}^{N}(\theta_{\text{IMU},i} - \theta_{\text{AI},i})^2} \tag{3.24}$$

where N represents the number of samples included in the comparison.

During the stable hold near the target position, the mean IMU-derived angle will also be compared with the corresponding angle obtained from OpenCap. Both the signed and absolute differences will be calculated.

The signed error will be defined as:

$$e_{\text{signed}} = \theta_{\text{IMU}} - \theta_{\text{AI}} \tag{3.25}$$

while the absolute error will be:

$$e_{\text{abs}} = |\theta_{\text{IMU}} - \theta_{\text{AI}}| \tag{3.26}$$

These tests will therefore evaluate the amplitude of the main movement, possible cross-talk in the other joint variables, and the agreement between the IMU-based reconstruction and the external video-based reference.

Functional task A2: hand-to-mouth

For the hand-to-mouth task, the three-dimensional trajectory of the wrist reconstructed from the kinematic model will be analysed.

Starting from the N-pose, the participant will lightly touch the centre of the lips with the same finger and then return to the initial position. Head and trunk movements will be kept as limited as possible during the execution.

The mouth will be used as a consistent functional target. However, it will not be considered a direct three-dimensional reference for the reconstructed wrist position, since physical contact occurs at the finger rather than at the wrist.

Each repetition will be analysed from the beginning of the movement until the return to the initial position. Since movement duration may vary between repetitions, each trajectory will be temporally normalised between 0% and 100% of the movement duration.

For each participant and side, the mean three-dimensional wrist trajectory across the five repetitions will be calculated.

Movement repeatability will then be evaluated by calculating the three-dimensional distance between each individual trajectory and the mean trajectory. This difference will be summarised using an RMS measure:

$$RMSE_{\text{traj}} = \sqrt{\frac{1}{N}\sum_{i=1}^{N} \|\mathbf{p}_i - \overline{\mathbf{p}}_i\|^2} \tag{3.27}$$

where $\mathbf{p}_i$ represents the wrist position of a single repetition and $\overline{\mathbf{p}}_i$ represents the corresponding point of the mean trajectory.

Lower values will indicate greater similarity between repetitions.

The repeatability of the position reached during the hand-to-mouth phase will also be evaluated. For each repetition, the wrist position around the maximum elbow flexion will be used as an approximate temporal reference for the terminal phase of the gesture.

The dispersion of the five terminal wrist positions around their mean position will then be calculated. This outcome will describe how consistently the participant reaches a similar reconstructed wrist position across repeated executions.

When a reliable three-dimensional wrist trajectory can be obtained from OpenCap tracking system, it will also be compared with the IMU-reconstructed trajectory after temporal and spatial alignment.

The A2 task will therefore mainly evaluate the repeatability of the reconstructed movement and, when possible, its consistency with the external video-based reconstruction.

Midline reach B1

The B1 task evaluated the reconstructed wrist position during reaching movements towards three anatomical targets along the body midline: the chest, mouth and forehead. Particular attention was given to the vertical position of the wrist.

The trunk IMU, identified as TO and positioned on the sternum, defined the origin of the reconstruction. The chest target was located at the level of TO. The initial resting position, with the arm extended alongside the body, was therefore distinct from the spatial origin.

Following a synchronisation gesture, the participant performed three repetitions on each side. Each repetition consisted of starting from rest, touching the chest, mouth and forehead in sequence, briefly maintaining each position, and returning to rest. Trunk movement was kept as limited as possible.

For a reconstructed wrist position relative to TO:

$$\mathbf{p}_w^{\mathrm{TO}} = \begin{bmatrix} x_w \\ y_w \\ z_w \end{bmatrix}, \tag{3.28}$$

the coordinate z_w represented wrist height along the gravity-defined vertical direction.

The reference heights were obtained from vertical anatomical distances measured using a tape:

$$\begin{aligned} z_{\mathrm{chest}}^{\mathrm{ref}} &= 0, \\ z_{\mathrm{mouth}}^{\mathrm{ref}} &= h_{\mathrm{TO-mouth}}, \\ z_{\mathrm{forehead}}^{\mathrm{ref}} &= h_{\mathrm{TO-mouth}} + h_{\mathrm{mouth-forehead}}. \end{aligned} \tag{3.29}$$

The analysis focused on the stable phase at each target. For each repetition, the mean reconstructed wrist height $\overline{z}_{w,k}$ was compared with the corresponding reference height:

$$e_{z,k} = \overline{z}_{w,k} - z_k^{\mathrm{ref}}, \tag{3.30}$$

where k identifies the chest, mouth or forehead target. Positive values indicated a reconstructed position above the reference, while negative values indicated a position below it.

The three repetitions allowed both agreement with the measured heights and repeatability of the reconstructed positions to be assessed. Wrist trajectories were also compared with those derived from OpenCap, considering three-dimensional position and vertical displacement.

During the same task, the behaviour of the virtual slave arm was observed. In mirror mode, the slave was expected to reproduce the reflected master configuration across the sagittal plane of the trunk.

This observation concerned the consistency of the simulated master-slave relationship.

Statistical analysis

For each participant, side, task and outcome, the five repetitions will first be analysed individually and subsequently summarised using the intra-subject mean and standard deviation.

For the A1 tasks, the IMU-derived angles will be compared with the corresponding angles obtained from the AI-based human pose tracking system.

The main comparison outcomes will include:

- ROM difference;
- signed angular error;
- absolute angular error;
- RMSE between the angular trajectories;
- cross-talk of the non-target joint variables.

The signed error will indicate whether the IMU-based model tends to overestimate or underestimate the external reference, while the absolute error will describe the overall magnitude of the difference independently of its direction.

For A2, the main outcomes will be the repeatability of the reconstructed wrist trajectory and the dispersion of the wrist position during the terminal hand-to-mouth phase.

When a reliable OpenCap wrist trajectory is available, the difference between the IMU-based and video-based trajectories will also be evaluated.

For B1, the main outcome will be the vertical and lateral deviation of the reconstructed wrist from the trunk midline for each of the three targets. The reconstructed wrist position will also be compared with the external geometrical reference and, when available, with the OpenCap derived wrist position.

After the subject-level analysis, the results will also be summarised at group level.

For each task and side, the mean value obtained from the five repetitions of each participant will be used as the participant-level value. Group results will then be reported as mean and standard deviation.

If the distributions are strongly asymmetric, the median and interquartile range will also be reported.

Right and left trials will be analysed separately in order to identify possible differences associated with the change of master side. These differences will not automatically be interpreted as measurement errors, since physiological asymmetry, movement strategy and sensor placement may also contribute to the observed variability.

If the sensors are removed and repositioned during the experimental protocol, the results obtained before and after repositioning will also be compared. This analysis will pro-

vide an indication of the sensitivity of the system to sensor replacement and repeated calibration.

Overall, the different tasks will evaluate complementary aspects of the proposed system. A1 will assess joint-angle reconstruction and agreement with the OpenCap external reference; A2 will evaluate the repeatability of the reconstructed functional movement; and B1 will assess the spatial consistency of the wrist reconstruction during midline reaching

4 | Results

4.1. Analyzed sample

The evaluation of six participants, P01, P02, P04, P05, P06 and P07, highlights three findings of particular interest: the close temporal agreement between the angular reconstructions, the repeatability of the master movement, and the possibility of transferring its geometry to a contralateral reference. The simulation brings these elements together within a coherent bimanual representation.

For A1 and A2, 44 blocks were documented, of which 43 were evaluable, comprising 202 repetitions. As both shoulder and elbow angles were examined in A2, the dataset included 51 angular comparison series. B1 comprised 12 recordings, with three sequences per side and participant, giving 36 sequences and 108 contacts with anatomical targets. Table **??** reports the trials actually analyzed. These numbers describe the available experimental sample.

Task	Participants	Evaluable blocks	Repetitions
A1.1	6	12	60
A1.2	6	12 (3 partial)	50
A1.3	6	11 (1 partial)	52
A2	4	8	40
B1	6	12	36 sequences

Table 4.1: Trial coverage and number of analyzed repetitions

Group summaries were obtained by first averaging the available sides within each participant and then assigning equal weight to each participant. For A1 and A2, the main summaries include complete blocks; partial recordings are retained in the individual results. P05 left A1.3 was not evaluable because the movement sequences could not be matched temporally. In B1, the P01 right comparison remains provisional because its

misalignment could not be adequately described by a single time delay; the IMU signal remains usable for comparison with the anatomical target heights.

Unless explicitly calculated, RMSE denotes the discrepancy between IMU and OpenCap reconstructions. The absolute comparison preserves the original references. The initial-posture comparison subtracts each signal's own mean over the same initial resting window. The centered RMSE instead removes the mean difference throught the entire windows

4.2. Angular agreement

Shoulder elevation generally showed closer agreement than the absolute elbow flexion values. Across participants with complete blocks, mean absolute RMSE was 9.91° for A1.1 and 7.75° for A1.2, with centred RMSE values of 5.43° and 5.48°, respectively. In A1.1 and A1.2, the comparison considers geometric arm elevation during movements performed respectively in the sagittal or frontal plane.

Task	n	**Absolute RMSE (°)**	**Initial RMSE (°)**	**Centred RMSE (°)**	**ΔROM (°)**
A1.1 shoulder	6	9.91 ± 2.48	8.68 ± 3.41	5.43	4.37
A1.2 shoulder	5	7.75 ± 1.10	9.55 ± 1.79	5.48	8.11
A1.3 elbow	6	25.79 ± 9.32	11.56 ± 3.51	8.81	-17.21
A2 shoulder	4	10.14 ± 1.50	9.83 ± 2.82	6.88	13.97
A2 elbow	4	27.08 ± 2.94	13.36 ± 1.91	9.25	-19.32

Absolute and initial-posture RMSE are reported as mean ± SD across participants. ΔROM was calculated as IMU ROM − OpenCap ROM. Centred RMSE and ΔROM are reported as mean values.

Table 4.2: Angular summary for complete blocks.

For elbow flexion in A1.3, mean absolute RMSE was 25.79°, decreasing to 11.56° when the signals were expressed relative to their initial posture. A similar reduction occurred for the elbow in A2, from 27.08° to 13.36°. The corresponding centred RMSE values, 8.81° and 9.25°, nevertheless indicate that some disagreement remained after removing the mean offset. The ROM comparison also identified amplitude differences: mean IMU elbow excursion was smaller than MOT excursion by 17.21° in A1.3 and 19.32° in A2.

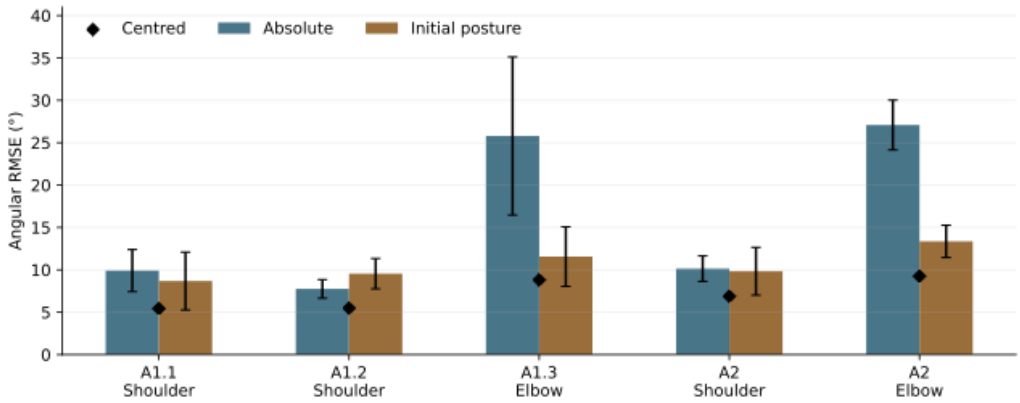

Figure 4.1: Absolute, initial-posture and centred angular RMSE. Bars and error bars show the mean and SD across participants after averaging their complete sides. Black symbols indicate mean centred RMSE. Sample sizes and values are reported in Table 4.2.

Temporal agreement was a recurring finding. The correlation coefficients in complete trials ranged from 0.9859 to 0.9986 for A1.1, from 0.9927 to 0.9971 for A1.2, and from 0.9894 to 0.9978 for A1.3. The inertial reconstruction therefore captured the phases of isolated movements consistently, even when absolute values differed.

Individual comparisons

Table 4.3 presents all available sides for the isolated movements. The individual analysis identifies both recordings with close agreement and conditions in which differences in reference or amplitude have a greater influence. Partial blocks are explicitly marked and are not treated as complete recordings.

Master side	A1.1 shoulder (°)	A1.2 shoulder (°)	A1.3 elbow (°)
P01 L	6.11 → 12.21 / 5.36	5.98 → 8.10 / 5.11	33.49 → 15.74 / 11.51
P01 R	9.89 → 10.53 / 6.93	7.37 → 13.53 / 6.88 *	22.37 → 11.15 / 8.98
P02 L	11.30 → 2.29 / 2.24	8.44 → 15.24 / 6.26	29.47 → 13.38 / 13.13
P02 R	15.72 → 5.13 / 5.09	7.57 → 6.83 / 5.51	20.36 → 13.48 / 12.41
P04 L	8.93 → 15.73 / 8.83	8.81 → 12.83 / 8.81 *	32.40 → 15.79 / 7.30
P04 R	7.98 → 6.55 / 3.76	9.25 → 16.38 / 8.82 *	38.75 → 9.07 / 7.50
P05 L	12.30 → 8.41 / 8.36	12.37 → 10.00 / 7.04	N/E
P05 R	6.25 → 5.95 / 5.34	5.16 → 9.88 / 5.09	34.82 → 15.12 / 10.14
P06 L	5.02 → 8.27 / 4.12	7.09 → 11.32 / 6.31	20.50 → 12.08 / 8.67
P06 R	10.36 → 4.57 / 4.20	9.90 → 11.40 / 6.75	21.08 → 6.84 / 5.54
P07 L	14.87 → 14.14 / 6.93	9.45 → 10.01 / 3.79	10.72 → 5.50 / 5.21
P07 R	10.15 → 10.42 / 3.96	5.55 → 4.58 / 3.86	12.12 → 7.47 / 4.53 *

Each cell: absolute → initial-posture / centred RMSE, in degrees. L = left; R = right. * Partial block. N/E = not evaluable.

Table 4.3: Isolated-movement RMSE by participant and side

Among the strongest cases of absolute shoulder agreement, P06 left A1.1 showed an RMSE of 5.02° and an MAE of 4.16°, while P05 right A1.2 showed an RMSE of 5.16° and an MAE of 4.58°. In P02 left A1.1, RMSE decreased from 11.30° to 2.29° after initial-posture subtraction, with a centred RMSE of 2.24° and a correlation coefficient of 0.9986. ROM in the same trial was 90.28 ± 2.61° for IMU and 93.26 ± 2.99° for OpenCap. This case demonstrates close agreement in angular change despite a difference in the absolute reference.

P04 right A1.1 yielded ROM values of 90.43 ± 1.88° for IMU and 90.55 ± 1.68° for OpenCap: a mean difference of only 0.12°, accompanied by low variability. This is a particularly good example of excursion reconstruction, although the absolute RMSE over the entire curve remained 7.98°. For the elbow, P07 left A1.3 achieved an initial-posture RMSE of 5.50° and a centered RMSE of 5.21°, with an absolute RMSE of 10.72°.

Differences between right and left sides did not follow a consistent direction. They include movement variability, separate calibrations and differences in the reference reconstruction.

4.3. Angular repetability

ROM repeatability was described by the standard deviation across repetitions within each block. Table 4.4 summarises the distribution of these SD values for complete blocks. This is a measure of within-session variability, encompassing both the participant's execution and the reconstruction; it does not estimate reproducibility after sensor repositioning.

Task	Blocks	IMU median (°)	IMU range (°)	OpenCap median (°)
A1.1 shoulder	12	2.66	1.31–4.06	3.01
A1.2 shoulder	9	3.29	1.60–5.13	2.84
A1.3 elbow	10	4.26	1.95–6.39	4.02
A2 shoulder	8	1.96	0.74–4.06	1.46
A2 elbow	8	2.10	0.96–2.60	2.55

The median is taken across individual block SD values.

Table 4.4: ROM SD in complete blocks

In A2, the SD of IMU elbow ROM ranged from 0.96° to 2.60°, with a median of 2.10°, below the MOT median of 2.55°. The consistency of excursion during this functional task is a strength of the master reconstruction: the reconstructed movement remained regular across repetitions. In A1.3, the median IMU SD was 4.26°, close to the MOT value of 4.02°. The favourable finding therefore concerns within-recording repeatability, which is distinct from anatomical accuracy.

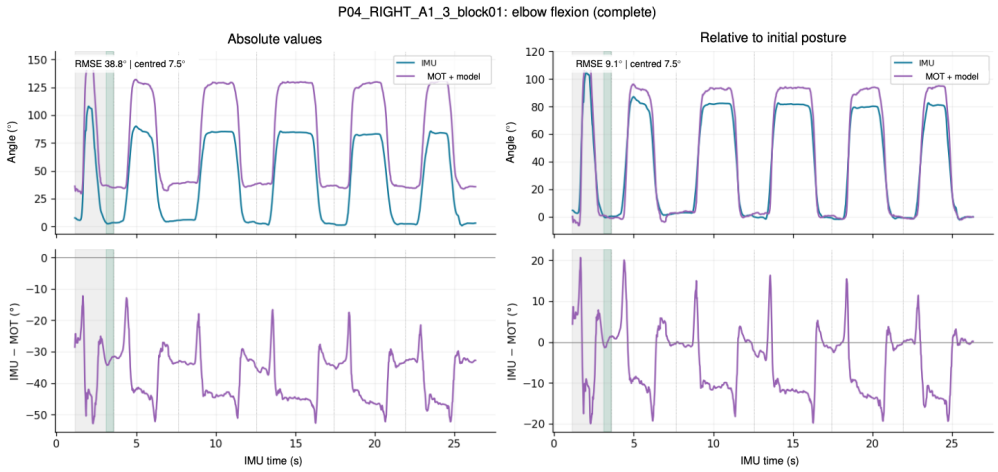

Figure 4.2: P04 right A1.3. Absolute and initial-posture angular comparisons, with IMU-OpenCap differences in the lower panels. RMSE decreases from 38.75° to 9.07°; centred RMSE remains 7.50°.

Figure 4.2 illustrates the influence of the angular zero. The five repetitions are clearly identifiable in both systems and the correlation coefficient is 0.9942, yet MOT retains substantial residual flexion in the lower posture. The IMU–MOT bias is −38.02°. A ROM difference of −12.31° remains after initial zeroing, confirming that the offset does not explain all disagreement. The operational cross-talk measure requires similar care because it includes movement actually performed in the non-target angle. Participant means across complete sides range from 5.58° to 18.32° in A1.1 and from 5.31° to 21.91° in A1.2; these values are not an isolated measure of sensor error.

4.4. Wrist trajectories and repeatability in A2

A2 trials were available for P01, P02, P06 and P07 on both sides. Wrist position was reconstructed through kinematic chains. In the absolute A2 comparison, coordinates are referenced to the shoulder of each model, with axes expressed in the trunk frame. The relative comparison describes displacement from each reconstruction's own initial posture.

Side	Absolute 3D (mm)	Initial 3D (mm)	Centred 3D (mm)	Absolute shoulder (°)	Absolute elbow (°)
P01 L	133.9	225.9	127.2	6.83	32.54
P01 R	132.8	102.5	66.2	9.63	22.77
P02 L	119.6	168.3	84.6	6.71	21.01
P02 R	179.7	245.5	162.8	12.60	32.09
P06 L	144.6	155.8	119.1	14.22	23.10
P06 R	196.5	253.9	159.1	8.15	38.13
P07 L	91.0	113.6	66.5	16.20	19.36
P07 R	109.4	155.0	96.6	6.74	27.63

The three 3D columns report position RMSE; the last two columns report angular RMSE. The absolute spatial comparison refer to to each model's shoulder.

Table 4.5: A2 comparisons for all available sides

The lowest absolute three-dimensional RMSE was observed in P07 left, at 90.99 mm, and the highest in P06 right, at 196.54 mm. Their centred RMSE values were 66.53 and 159.10 mm, respectively. In seven of the eight sides, the initial-posture comparison produced a higher 3D RMSE than the absolute comparison: aligning the resting positions did not automatically align the paths.

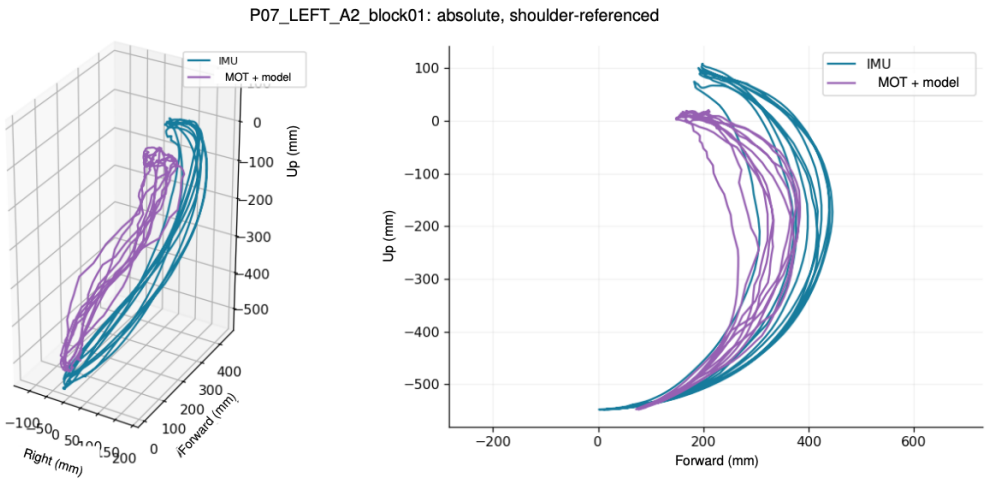

Figure 4.3: A2 trajectories for P07 LEFT, the case with the lowest absolute 3D RMSE. The left panel shows the three-dimensional reconstruction and the right panel its forward-upward projection.

Three-dimensional dispersion of IMU terminal postures ranged from 15.18 to 32.22 mm,

while the jitter during the hold ranged from 2.48 to 10.56 mm. In P07 left, dispersion was 17.13 mm for IMU and 21.20 mm for MOT, providing a good example of spatial repeatability. These results describe master stability.

4.5. Contacts heights in B1

In B1, the origin is located at the TO sensor on the sternum. The movement begins at rest, with the arm extended at the side of the body; this configuration has its own coordinates and does not coincide with the origin. Chest contact is referenced to the height of TO. Mouth and forehead heights are participants specific.

Side	Absolute 3D (mm)	Initial 3D(mm)	Centred 3D(mm)	Absolute Z(mm)	Centred Z(mm)
P01 L	107.4	83.6	66.6	45.3	20.9
P01 R *	251.8	726.5	212.4	188.6	176.2
P02 L	167.6	211.0	143.7	100.7	59.0
P02 R	147.6	175.6	118.9	87.0	47.6
P04 L	154.4	183.2	123.2	79.1	38.8
P04 R	105.8	77.2	54.4	35.2	18.9
P05 L	182.7	235.4	147.2	105.6	63.0
P05 R	86.8	117.0	78.3	31.0	17.6
P06 L	154.9	155.8	94.6	88.0	55.8
P06 R	148.8	128.6	74.6	58.5	48.4
P07 L	93.3	108.6	76.7	47.8	28.4
P07 R	118.2	110.5	82.1	34.3	25.6

Z RMSE refers to the full analyzed trajectory, not only the contacts.

Table 4.6: B1 trajectory RMSE

In verified comparisons, absolute 3D RMSE ranged from 86.79 mm in P05 right to 182.67 mm in P05 left. Vertical discrepancies were smaller in several sides: Z RMSE was 31.02 mm in P05 right, 34.30 mm in P07 right and 35.20 mm in P04 right. Their centered vertical RMSE values were 17.65, 25.64 and 18.94 mm, respectively. These results identify conditions in which the systems closely reproduced the progression in height.

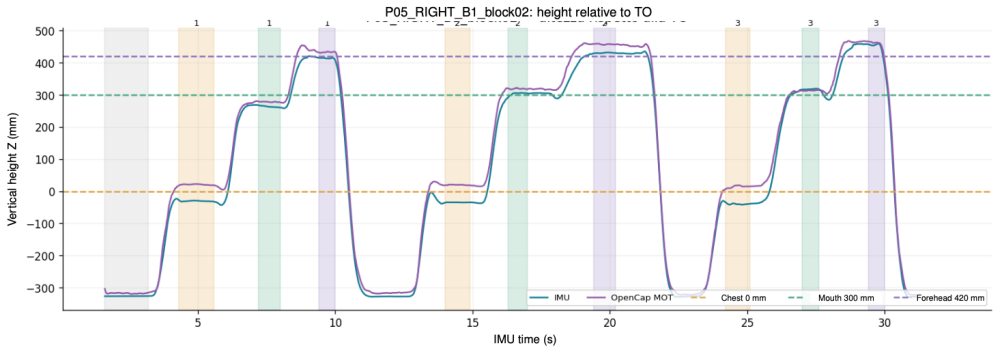

Figure 4.4: P05 right B1. Wrist height relative to TO and the external chest, mouth and forehead references. Shaded bands identify the contact windows.

The estimated TO position in OpenCap and the unmeasured anterior-posterior distance between the sternum and the shoulder midpoint also limit the interpretation of absolute 3D discrepancies.

Lateral alignment during B1

The lateral wrist coordinate provided further evidence of the reconstruction's ability to represent midline reaching. In P01 left, the mean wrist positions during the three forehead holds were −5.32, 3.60 and 1.64 mm along the X axis, corresponding to a mean absolute lateral distance of only 3.52 mm from the model midline. The reconstructed wrist therefore remained essentially centred during these holds, consistent with the graphical representation.

Close lateral alignment was also observed in other participant-target combinations. The mean absolute lateral distance across the three holds was 3.10 mm for P02 left at the chest, 5.05 mm for P04 right at the forehead and 6.08 mm for P07 left at the mouth. These findings demonstrate that the reconstruction reproduce target positions close to the body midline.

4.6. Intra-patients analisys

Across participants, the closest agreement was observed in different tasks. Some showed better agreement for shoulder movements, while others had more consistent elbow movements or closer wrist positions. No participant showed the best results in all comparisons.

For shoulder movements, P02 left achieved particularly close agreement in A1.1 after initial-posture subtraction, with an RMSE of 2.29°. P04 right reproduced almost the same ROM as OpenCap, with a difference of only 0.12°. Good absolute agreement was

also observed in P06 left A1.1 and P05 right A1.2, with RMSE values of 5.02° and 5.16°, respectively. The strongest shoulder results therefore involved several participants rather than a single recording.

For the elbow, P07 left showed the lowest absolute RMSE among complete A1.3 blocks. The same side also had the lowest absolute 3D RMSE in A2. P01 right stood out for repeatability during A2, with an elbow ROM SD of 0.96°. These results highlight different strengths: close agreement with OpenCap in P07 and consistent excursion across repetitions in P01.

In B1, P05 right reproduced the measured mouth and forehead heights closely. P02 showed larger differences at the chest, despite the good shoulder agreement in A1.1. P07 also showed differences in mouth height, even though its A1.3 and A2 results were among the closest to OpenCap.

Taken together, these findings show that the reconstruction performed well in several participants, although the results depended on the task. Good agreement in joint angles did not always correspond to equally close wrist positions. The agreement and repeatability observed provide a useful basis for the bimanual simulation, while absolute wrist positioning remains an area for improvement across participants.

5 | Discussion

5.1. Basis of bimanual simulation

The main contribution of this work is the development of a system that uses three IMUs to reconstruct the master arm and generate a contralateral movement reference. The experimental results showed consistent angular profiles, repeatable excursions and recognisable functional postures, supporting the use of the reconstructed movement as the input to the bimanual simulation.

Temporal agreement with OpenCap was consistently high across the isolated movements, with correlation coefficients ranging from approximately 0.986 to 0.999 in complete blocks. The shoulder results provided several examples of close agreement. In P02 left A1.1, RMSE relative to the initial posture was 2.29°, with a centred RMSE of 2.24°. P04 right A1.1 showed a ROM difference of only 0.12°, while P06 left achieved an absolute RMSE of 5.02°. These findings demonstrate agreement in different aspects of the movement, although performance varied across participants and recordings. OpenCap provides a useful comparison baseline, but discrepancies cannot be attributed solely to the IMU algorithm. OpenCap values depend on the underlying joint model and its coordinate conventions, whereas the inertial reconstruction combines segment orientations, calibration and anthropometric measurements. RMSE therefore describes the difference between the two estimates without establishing which is closer to the anatomical movement. Initial references, movement amplitudes and curve profiles must also be considered when interpreting the results.

The wrist analysis added information about spatial consistency. Repeatable terminal postures in A2 and favourable agreement with measured heights in specific B1 recordings showed that the system could reproduce relevant features of functional movements. Absolute wrist positioning was more variable, identifying geometric calibration as an important area for improvement. These findings are directly relevant to the bimanual simulation, where the slave reference is generated from the reconstructed master. Reflection across the trunk sagittal plane preserves segment lengths and the geometric elbow angle while

reversing laterality. For a common reference frame and reflection plane, the relationship $\mathbf{e}_{\text{slave}} = \mathbf{S}\mathbf{e}_{\text{master}}$ also preserves the norm of the reconstruction discrepancy. Ideal mirroring therefore transfers the movement without amplifying the master's spatial error, so improvements in its reconstruction directly benefit the contralateral reference.

The framework was used with both right and left masters, supporting its application to either active side. The experimental results and the geometric properties of mirroring together provide a basis for simulated bimanual control. Dedicated measurements of slave trajectories and latency are still required to verify the implementation quantitatively. Future integration with an exoskeleton can build on this approach by adapting the reference to the user's mobility and the device's joint coordinates and mechanical limits.

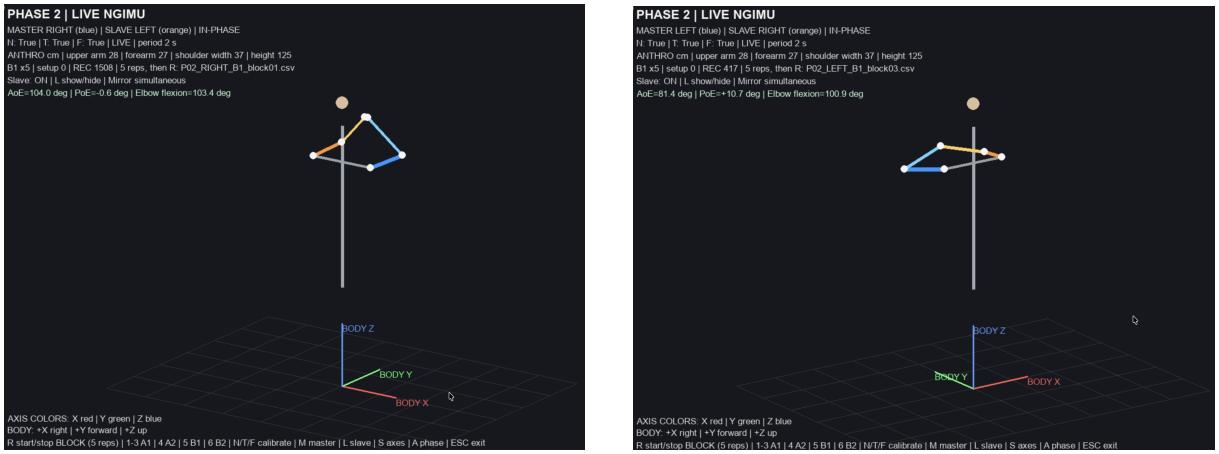

(a) Right arm as master (b) Left arm as master

Figure 5.1: Bimanual simulation with the right and left arms alternately acting as the master. The virtual slave reproduces the reflected master configuration across the trunk sagittal plane.

5.2. Elbow reconstruction and differences from OpenCap

The elbow results show why absolute agreement and movement pattern need to be considered separately. Both systems captured similar flexion and return phases, as indicated by the high correlations, but often assigned different angular values to the same posture. After subtracting the initial posture, mean RMSE decreased by more than half in A1.3 and by approximately half in A2. This suggests that differences in the starting reference represents a substantial part of the disagreement. P04 right A1.3 illustrates this clearly. During the lower hold, OpenCap retained a noticeable flexion angle, while the IMU recon-

struction remained close to its calibrated extension reference. Absolute RMSE was 38.75°, but decreased to 9.07° when the signals were compared to their initial posture, with a correlation coefficient of 0.9942. The difference therefore cannot be attributed entirely to the inertial algorithm.

These observations also raise the possibility that the IMU reconstruction represents elbow posture more faithfully in some conditions. Elbow flexion is calculated from the relationship between the calibrated longitudinal directions of the upper arm and forearm, providing a direct geometric description of their relative position.

Differences in movement amplitude remained even after accounting for the initial reference. Mean IMU elbow ROM was lower than OpenCap ROM by 17.21° in A1.3 and 19.32° in A2. Since subtracting a constant offset does not change ROM, these differences may arise from axis calibration, joint definitions or the reconstruction models.

Repeatability nevertheless provides favourable evidence for the IMU approach. In A2, the median SD of elbow ROM was 2.10° for IMU and 2.55° for OpenCap, with an IMU value of only 0.96° in P01 right. P07 left A1.3 also showed close agreement relative to the initial posture, with an RMSE of 5.50°. These results support the use of the reconstructed elbow movement in the simulation: the signal followed the gesture consistently and reproduced similar excursions across repetitions. They also show why a larger absolute difference from OpenCap should not be taken as evidence of poorer reconstruction.

5.3. Spatial reconstruction: repeatability and limitations

The spatial results show that repeatability and agreement between systems describe different aspects of the reconstruction. In A2, IMU terminal postures had a 3D dispersion of approximately 15–32 mm, with fluctuations during the holds of approximately 2.5–10.6 mm. These values indicate that the master could reproduce similar positions across repetitions, even when the full trajectories differed more substantially from OpenCap. For the bimanual simulation, this consistency is a useful outcome.

B1 provided additional evidence through the measured anatomical heights. P05 right showed an IMU–OpenCap vertical RMSE of 31.02 mm and RMSE values against the targets of 23.49 mm at the mouth and 16.58 mm at the forehead. In P01 left, IMU height biases were also smaller than the corresponding OpenCap values at both targets. These cases demonstrate the potential of the reconstruction, although OpenCap had lower mean absolute errors across participants. The main challenge is to achieve similarly close

positioning more consistently across recordings.

Some spatial differences may arise from the reference definitions as well as the reconstructed movement. Head and trunk motion can change the target heights, the reconstructed wrist does not necessarily coincide with the anatomical contact point, and TO was estimated geometrically in OpenCap. The chest results for P04 and P06 illustrate this distinction: vertical SD values below 5 mm occurred with biases above 60 mm.

This findings should also be considered a preliminary technical evaluation. Six participants were assessed, missing samples reduced coverage in some recordings, while retrospective synchronization enabled comparison without measuring the actual system latency. Differences in model scaling, joint origins and acquisition posture also contributed to variability between participants. These factors limit the extent to which every discrepancy can be attributed to the IMU algorithm.

Overall, the study provides a working reconstruction with good agreement and repeatability in several conditions, together with a geometrically consistent basis for bimanual reference generation. Further validation should examine sensor repositioning, recordings across different days, exported slave trajectories and latency. These steps would strengthen the current findings and support the transition to an exoskeleton, where accurate positioning, device tracking and interaction with the user will require dedicated evaluation.

6 | Conclusion

6.1. Main findings

This thesis developed a master-slave framework that uses three IMUs to reconstruct upper-limb movement and generate a contralateral reference. The system combines sensor-to-segment calibration, kinematic reconstruction and a three-dimensional representation of both arms. Its main contribution is the integration of these components into a working bimanual simulation, in which the voluntary movement of either arm can guide the virtual opposite limb.

The evaluation in six participants showed a positive agreement with OpenCap in several conditions. Correlations were consistently high during isolated movements, and mean absolute shoulder RMSE was 9.91° in A1.1 and 7.75° in A1.2. Individual recordings showed closer agreement, including an RMSE of 2.29° relative to the initial posture and a ROM difference of only 0.12°. These results indicate that the reconstruction could capture both the progression and amplitude of the movement, although agreement varied across participants and tasks.

The elbow results highlighted the importance of the angular reference. In A1.3, mean RMSE decreased from 25.79° to 11.56° after initial-posture subtraction. Elbow excursion was also repeatable during A2, with a median ROM SD of 2.10° for IMU, compared with 2.55° for OpenCap. These findings show that a large absolute difference from OpenCap does not necessarily imply poor reconstruction of the movement itself.

The spatial results provided further evidence of consistency. Terminal wrist positions in A2 had a dispersion of approximately 15–32 mm, while specific B1 recordings showed close agreement with the measured anatomical heights. Absolute wrist positioning was less uniform across participants, indicating that geometric calibration remains an important area for improvement.

The mirror transformation provides a defined relationship between the reconstructed master and the virtual slave. It preserves segment lengths and geometric joint angles without

amplifying the master's Euclidean reconstruction discrepancy. Together, the experimental findings and these geometric properties support the feasibility of the bimanual simulation. The work therefore establishes a basis for future IMU-exoskeleton integration, while remaining a preliminary technical evaluation rather than a demonstration of physical assistance or rehabilitation efficacy.

6.2. Future development

The next stage is to improve the consistency of the reconstruction and implement the master-slave paradigm to a physical exoskeleton. For the master, priorities include more repeatable anthropometric measurements, clearer correspondence between anatomical landmarks and model points, and systematic checks of the calibration poses. Repeating the tests after sensor repositioning and on different days would establish whether the performance observed within individual recordings is maintained across sessions.

Independent reference measurements would also strengthen the evaluation. Known joint angles during maintained postures could help clarify the elbow differences observed between IMU and OpenCap. Spatial targets measured in the same coordinate system as the reconstruction would provide a more direct assessment of wrist positioning. Both absolute and initial-posture comparisons should be considered, as they describe different aspects of agreement.

For exoskeleton integration, the mirrored movement must be converted into joint commands compatible with the device and the user's available range of motion. Movement amplitude and speed may need to be adapted rather than reproduced directly. Position feedback will be necessary to distinguish the desired reference from the movement actually performed, while appropriate limits and signal-loss handling must be incorporated into the controller.

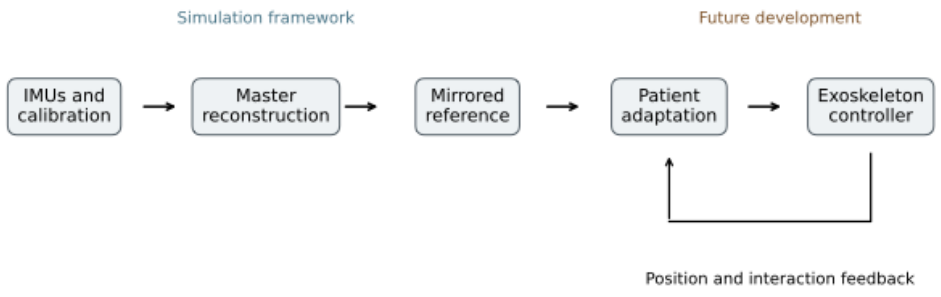

Figure 6.1: Pipeline development towards an IMU-exoskeleton system.

The longer-term objective is to use voluntary movement of the master arm to guide personalized assistance of the opposite limb. The present simulation provides the kinematic basis for this approach. Further development should preserve this clear relationship between the two limbs while introducing the adaptation, feedback and experimental validation needed for physical assistance.

Bibliography

[1] T. Alves et al. Serious games strategies with cable-driven robots for bimanual rehabilitation: A randomized controlled trial with post-stroke patients. *Frontiers in Robotics and AI*, 9:739088, 2022.

[2] E. Bardi et al. Upper limb soft robotic wearable devices: a systematic review. *Journal of NeuroEngineering and Rehabilitation*, 19:87, 2022.

[3] E. Bardi et al. 3d upper limbs tracking through inertial sensors: calibration, methodology, and validation. In *GNB 2023*, Padova, Italy, 2023.

[4] K. Boardsworth et al. Upper limb robotic rehabilitation following stroke: a systematic review and meta-analysis investigating efficacy and the influence of device features and program parameters. *Journal of NeuroEngineering and Rehabilitation*, 22:164, 2025.

[5] B. C. V. Campbell et al. Ischaemic stroke. *Nature Reviews Disease Primers*, 5(1): 70, 2019.

[6] J. H. Cauraugh and S. Kim. Two coupled motor recovery protocols are better than one: Electromyogram-triggered neuromuscular stimulation and bilateral movements. *Stroke*, 33:1589–1594, 2002.

[7] J. Chen et al. Robot-assisted mirror rehabilitation for post-stroke upper limbs: A personalized control strategy. *Sensors*, 25:5659, 2025.

[8] S. M. Christopher and M. J. Johnson. Task-oriented robot-assisted stroke therapy of paretic limb improves control in a unilateral and bilateral functional drink task: A case study. In *Annual International Conference of the IEEE Engineering in Medicine and Biology Society*, pages 1194–1197, 2014.

[9] A. M. Cinnera et al. Upper limb assessment with inertial measurement units according to the international classification of functioning in stroke: a systematic review and correlation meta-analysis. *Topics in Stroke Rehabilitation*, 31(1):66–85, 2024.

[10] E. S. Donkor. Stroke in the 21st century: A snapshot of the burden, epidemiology, and quality of life. *Stroke Research and Treatment*, 2018:3238165, 2018.

[11] E. Gerardin et al. Bimanual motor skill learning with robotics in chronic stroke: comparison between minimally impaired and moderately impaired patients, and healthy individuals. *Journal of NeuroEngineering and Rehabilitation*, 19:28, 2022.

[12] M. Karasheva et al. Sensor-driven control strategies for post-stroke shoulder rehabilitation exoskeletons: A systematic review. *MethodsX*, 15:103648, 2025.

[13] P. Kiper et al. Proprioceptive based training for stroke recovery. proposal of new treatment modality for rehabilitation of upper limb in neurological diseases. *Archives of Physiotherapy*, 5:6, 2015.

[14] T. M. Kwok and H. Yu. A novel bilateral underactuated upper limb exoskeleton for post-stroke bimanual adl training. *IEEE Transactions on Neural Systems and Rehabilitation Engineering*, 32:3299–3309, 2024.

[15] K. Little et al. Imu-based assistance modulation in upper limb soft wearable exosuits. In *2019 IEEE 16th International Conference on Rehabilitation Robotics (ICORR)*, pages 1197–1202, 2019.

[16] Y. Liu et al. Bimanual coordination in individuals post-stroke: Constraints, rehabilitation approaches and measures: Systematic review. *International Journal of Exercise Science*, 17(3):831–851, 2024.

[17] D. Ma et al. Robot-assisted bimanual training improves hand function in patients with subacute stroke: A randomized controlled pilot study. *Frontiers in Neurology*, 13:884261, 2022.

[18] B. Sheng et al. Bilateral robots for upper-limb stroke rehabilitation: State of the art and future prospects. *Medical Engineering & Physics*, 38(7):587–606, 2016.

[19] C. Tang et al. Bilateral upper limb robot-assisted rehabilitation improves upper limb motor function in stroke patients: a study based on quantitative eeg. *European Journal of Medical Research*, 28:603, 2023.

[20] T. Triwiyanto et al. Bilateral mode exoskeleton for hand rehabilitation with wireless control using 3d printing technology based on imu sensor. *HardwareX*, 14:e00432, 2023.

A | Appendix A

Tables and overall summary

L = left; R = right. Angular values are in degrees; spatial values are in millimetres. Abs. preserves the original reference. Init. subtracts each signal's own initial-rest mean. Cent. removes the mean inter-system difference over the analysed window and is descriptive, not independently calibrated accuracy. Inter-system bias and ROM differences use IMU minus MOT; target-height bias uses reconstruction minus measured reference. SD denotes standard deviation. N/E = not evaluable; N/A = unavailable. * marks partial A1 blocks.

Table A.1: Group angular agreement (degrees)

Task	n	RMSE abs.	RMSE init.	RMSE cent.	Bias abs.	ROM diff.
A1.1 shoulder	6	9.91 ± 2.48	8.68 ± 3.41	5.43 ± 1.27	-2.15	4.37
A1.2 shoulder	5	7.75 ± 1.10	9.55 ± 1.79	5.48 ± 1.06	1.71	8.11
A1.3 elbow	6	25.79 ± 9.32	11.56 ± 3.51	8.81 ± 2.73	-24.03	-17.21
A2 shoulder	4	10.14 ± 1.50	9.83 ± 2.82	6.88 ± 1.48	1.43	13.97
A2 elbow	4	27.08 ± 2.94	13.36 ± 1.91	9.25 ± 2.57	-25.25	-19.32

RMSE entries are mean ± between-participant SD; bias and ROM difference are means. A2 was available only for P01, P02, P06 and P07.

A.1. Test A1.1

Table A.2: Angular agreement: A1.1: shoulder elevation

Side	Reps	RMSE abs.	RMSE init.	RMSE cent.	Bias abs.	MAE abs.	r
P01 L	5	6.11	12.21	5.36	-2.93	4.43	0.9950
P01 R	5	9.89	10.53	6.93	-7.05	8.01	0.9948
P02 L	5	11.30	2.29	2.24	-11.08	11.08	0.9986
P02 R	5	15.72	5.13	5.09	-14.88	14.88	0.9972
P04 L	5	8.93	15.73	8.83	1.29	8.22	0.9947
P04 R	5	7.98	6.55	3.76	-7.03	7.43	0.9954
P05 L	5	12.30	8.41	8.36	9.03	10.58	0.9859
P05 R	5	6.25	5.95	5.34	-3.24	5.67	0.9920
P06 L	5	5.02	8.27	4.12	-2.88	4.16	0.9962
P06 R	5	10.36	4.57	4.20	-9.47	9.60	0.9963
P07 L	5	14.87	14.14	6.93	13.16	13.16	0.9907
P07 R	5	10.15	10.42	3.96	9.34	9.34	0.9941

All angular metrics are in degrees except r. Partial blocks are shown but excluded from the main group summary.

Table A.3: Excursion and repeatability: A1.1: shoulder elevation

Side	IMU ROM	OpenCap ROM	ROM diff.	Coverage (%)	Cross-talk
P01 L	92.14 ± 2.70	81.86 ± 4.28	10.28 ± 3.41	100.00	9.31 ± 2.12
P01 R	97.37 ± 3.58	85.45 ± 5.53	11.92 ± 3.35	97.65	5.33 ± 1.34
P02 L	90.28 ± 2.61	93.26 ± 2.99	-2.98 ± 2.65	100.00	11.61 ± 1.57
P02 R	82.91 ± 1.98	94.68 ± 3.03	-11.78 ± 3.01	100.00	10.13 ± 1.15
P04 L	102.52 ± 4.06	86.79 ± 8.09	15.73 ± 4.59	53.12	24.03 ± 2.48
P04 R	90.43 ± 1.88	90.55 ± 1.68	-0.12 ± 2.09	100.00	12.61 ± 0.59
P05 L	105.00 ± 1.53	92.88 ± 1.14	12.12 ± 1.74	75.95	14.35 ± 2.95
P05 R	98.86 ± 1.92	101.12 ± 3.95	-2.26 ± 2.60	100.00	13.18 ± 2.22
P06 L	97.42 ± 1.31	90.74 ± 1.78	6.68 ± 2.95	100.00	6.19 ± 1.68
P06 R	85.95 ± 2.73	90.74 ± 3.69	-4.79 ± 4.84	100.00	4.96 ± 1.52
P07 L	92.65 ± 3.17	79.42 ± 2.13	13.23 ± 2.57	99.45	7.08 ± 0.77
P07 R	86.39 ± 3.81	81.93 ± 1.85	4.46 ± 2.80	100.00	5.33 ± 0.99

ROM, paired ROM differences and cross-talk are mean ± within-block SD across repetitions, in degrees. Cross-talk is included for A1.1/A1.2 only and can contain genuine non-target movement. Coverage is the valid comparison-grid percentage; it is distinct from repetition count.

A.2. Test A1.2

Table A.4: Angular agreement: A1.2: shoulder elevation

Side	Reps	RMSE abs.	RMSE init.	RMSE cent.	Bias abs.	MAE abs.	r
P01 L	5	5.98	8.10	5.11	-3.12	4.64	0.9971
P01 R *	2	7.37	13.53	6.88	-2.65	5.99	0.9984
P02 L	5	8.44	15.24	6.26	-5.66	6.50	0.9960
P02 R	5	7.57	6.83	5.51	-5.20	5.57	0.9961
P04 L *	1	8.81	12.83	8.81	-0.25	7.92	0.9783
P04 R *	2	9.25	16.38	8.82	2.79	8.73	0.9980
P05 L	5	12.37	10.00	7.04	10.17	10.46	0.9948
P05 R	5	5.16	9.88	5.09	0.84	4.58	0.9971
P06 L	5	7.09	11.32	6.31	3.24	6.11	0.9927
P06 R	5	9.90	11.40	6.75	7.25	8.13	0.9945
P07 L	5	9.45	10.01	3.79	8.65	8.65	0.9947
P07 R	5	5.55	4.58	3.86	4.00	4.38	0.9970

All angular metrics are in degrees except r. Partial blocks are shown but excluded from the main group summary.

Table A.5: Excursion and repeatability: A1.2: shoulder elevation

Side	IMU ROM	OpenCap ROM	ROM diff.	Coverage (%)	Cross-talk
P01 L	88.46 ± 5.13	77.80 ± 4.18	10.66 ± 4.39	94.66	5.31 ± 0.93
P01 R *	91.96 ± 0.57	78.78 ± 0.83	13.17 ± 0.26	100.00	4.30 ± 0.30
P02 L	90.37 ± 3.58	79.02 ± 2.94	11.35 ± 2.27	100.00	23.61 ± 0.85
P02 R	90.38 ± 3.29	80.77 ± 2.68	9.61 ± 2.13	100.00	12.15 ± 4.18
P04 L *	83.96 ± –	71.30 ± –	12.66 ± –	52.20	21.50 ± –
P04 R *	90.69 ± 1.45	73.12 ± 2.69	17.57 ± 1.24	100.00	12.55 ± 0.56
P05 L	79.58 ± 2.91	65.81 ± 2.68	13.78 ± 1.66	75.56	15.52 ± 1.07
P05 R	88.18 ± 4.03	80.24 ± 4.82	7.94 ± 3.36	78.83	28.30 ± 2.30
P06 L	95.36 ± 4.45	86.40 ± 2.84	8.97 ± 3.44	99.06	6.85 ± 2.19
P06 R	95.48 ± 1.60	83.11 ± 3.99	12.37 ± 3.08	100.00	8.18 ± 1.32
P07 L	88.27 ± 1.70	86.49 ± 1.84	1.78 ± 2.46	100.00	6.82 ± 0.41
P07 R	90.34 ± 1.92	96.38 ± 1.38	-6.04 ± 2.62	100.00	12.04 ± 0.63

ROM, paired ROM differences and cross-talk are mean ± within-block SD across repetitions, in degrees. Cross-talk is included for A1.1/A1.2 only and can contain genuine non-target movement. Coverage is the valid comparison-grid percentage; it is distinct from repetition count.

A.3. Test A1.3

Table A.6: Angular agreement: A1.3: elbow flexion

Side	Reps	RMSE abs.	RMSE init.	RMSE cent.	Bias abs.	MAE abs.	r
P01 L	5	33.49	15.74	11.51	-31.45	31.45	0.9939
P01 R	5	22.37	11.15	8.98	-20.48	20.66	0.9930
P02 L	5	29.47	13.38	13.13	-26.39	26.68	0.9908
P02 R	5	20.36	13.48	12.41	-16.14	17.59	0.9895
P04 L	5	32.40	15.79	7.30	-31.57	31.57	0.9960
P04 R	5	38.75	9.07	7.50	-38.02	38.02	0.9942
P05 L	N/E	–	–	–	–	–	–
P05 R	5	34.82	15.12	10.14	-33.31	33.31	0.9978
P06 L	5	20.50	12.08	8.67	-18.57	18.59	0.9902
P06 R	5	21.08	6.84	5.54	-20.34	20.34	0.9894
P07 L	5	10.72	5.50	5.21	-9.37	9.62	0.9954
P07 R *	2	12.12	7.47	4.53	-11.24	11.24	0.9932

All angular metrics are in degrees except r. Partial blocks are shown but excluded from the main group summary.

Table A.7: Excursion and repeatability: A1.3: elbow flexion

Side	IMU ROM	OpenCap ROM	ROM diff.	Coverage (%)	Cross-talk
P01 L	74.49 ± 6.32	98.82 ± 4.83	-24.33 ± 2.64	98.57	–
P01 R	84.58 ± 3.46	101.39 ± 3.62	-16.81 ± 1.16	100.00	–
P02 L	88.24 ± 4.29	118.27 ± 6.27	-30.03 ± 6.18	100.00	–
P02 R	91.82 ± 2.06	116.57 ± 2.88	-24.75 ± 1.94	100.00	–
P04 L	87.63 ± 4.46	103.60 ± 2.69	-15.97 ± 2.23	53.49	–
P04 R	83.99 ± 1.95	96.30 ± 2.34	-12.31 ± 1.21	100.00	–
P05 L	–	–	–	–	–
P05 R	88.94 ± 4.23	112.90 ± 4.41	-23.95 ± 2.28	67.19	–
P06 L	84.60 ± 5.68	99.26 ± 2.29	-14.66 ± 6.09	100.00	–
P06 R	84.78 ± 6.39	88.90 ± 9.65	-4.12 ± 10.74	100.00	–
P07 L	81.53 ± 4.03	89.34 ± 5.00	-7.81 ± 1.75	100.00	–
P07 R *	86.19 ± 3.46	79.79 ± 1.90	6.41 ± 1.57	99.20	–

ROM, paired ROM differences and cross-talk are mean ± within-block SD across repetitions, in degrees. Cross-talk is included for A1.1/A1.2 only and can contain genuine non-target movement. Coverage is the valid comparison-grid percentage; it is distinct from repetition count.

P05 left A1.3 is not evaluable because the sequences could not be matched.

A.4. Test A2

Table A.8: Angular agreement: A2: shoulder elevation

Side	Reps	RMSE abs.	RMSE init.	RMSE cent.	Bias abs.	MAE abs.	r
P01 L	5	6.83	8.04	6.82	-0.22	6.38	0.9959
P01 R	5	9.63	11.45	7.58	-5.95	7.24	0.9936
P02 L	5	6.71	7.48	6.22	-2.54	5.44	0.9880
P02 R	5	12.60	4.46	4.39	-11.82	11.87	0.9722
P06 L	5	14.22	15.84	9.81	10.29	12.00	0.9951
P06 R	5	8.15	9.31	7.73	2.59	7.36	0.9907
P07 L	5	16.20	15.86	7.88	14.16	14.16	0.9890
P07 R	5	6.74	6.19	4.60	4.93	5.65	0.9879

All angular metrics are in degrees except r. Partial blocks are shown but excluded from the main group summary.

Table A.9: Excursion and repeatability: A2: shoulder elevation

Side	IMU ROM	OpenCap ROM	ROM diff.	Coverage (%)	Cross-talk
P01 L	68.46 ± 2.88	54.78 ± 1.68	13.67 ± 3.26	98.59	–
P01 R	64.51 ± 0.92	47.37 ± 1.13	17.14 ± 1.36	100.00	–
P02 L	66.20 ± 2.04	54.59 ± 2.47	11.61 ± 1.94	100.00	–
P02 R	46.77 ± 1.19	46.33 ± 1.43	0.44 ± 1.48	100.00	–
P06 L	92.90 ± 4.06	70.37 ± 1.23	22.53 ± 3.37	99.63	–
P06 R	66.90 ± 2.82	48.10 ± 1.50	18.80 ± 2.36	100.00	–
P07 L	66.47 ± 1.89	48.72 ± 1.54	17.75 ± 1.31	100.00	–
P07 R	59.90 ± 0.74	50.06 ± 0.68	9.84 ± 1.18	99.49	–

ROM, paired ROM differences and cross-talk are mean ± within-block SD across repetitions, in degrees. Cross-talk is included for A1.1/A1.2 only and can contain genuine non-target movement. Coverage is the valid comparison-grid percentage; it is distinct from repetition count.

Table A.10: Angular agreement: A2: elbow flexion

Side	Reps	RMSE abs.	RMSE init.	RMSE cent.	Bias abs.	MAE abs.	r
P01 L	5	32.54	16.74	8.24	-31.48	31.48	0.9972
P01 R	5	22.77	8.97	5.53	-22.08	22.08	0.9972
P02 L	5	21.01	11.99	10.05	-18.46	18.46	0.9923
P02 R	5	32.09	20.12	15.68	-28.00	28.01	0.9933
P06 L	5	23.10	18.17	10.30	-20.68	20.76	0.9919
P06 R	5	38.13	7.81	7.77	-37.33	37.33	0.9956
P07 L	5	19.36	10.48	8.01	-17.63	17.63	0.9927
P07 R	5	27.63	12.62	8.44	-26.31	26.31	0.9959

All angular metrics are in degrees except r. Partial blocks are shown but excluded from the main complete-block group summary.

Table A.11: Excursion and repeatability: A2: elbow flexion

Side	IMU ROM	OpenCap ROM	ROM diff.	Coverage (%)	Cross-talk
P01 L	95.73 ± 2.27	112.19 ± 2.31	-16.46 ± 1.20	98.59	–
P01 R	106.58 ± 0.96	117.30 ± 2.10	-10.72 ± 1.94	100.00	–
P02 L	115.06 ± 2.60	135.07 ± 2.80	-20.01 ± 2.95	100.00	–
P02 R	105.36 ± 2.17	141.08 ± 1.73	-35.72 ± 1.30	100.00	–
P06 L	91.94 ± 2.04	114.29 ± 3.95	-22.35 ± 5.07	99.63	–
P06 R	99.05 ± 1.83	117.24 ± 2.07	-18.19 ± 2.35	100.00	–
P07 L	110.12 ± 1.92	126.04 ± 3.45	-15.92 ± 2.01	100.00	–
P07 R	104.23 ± 2.24	119.42 ± 2.95	-15.19 ± 1.47	99.49	–

ROM, paired ROM differences and cross-talk are mean ± within-block SD across repetitions, in degrees. Cross-talk is included for A1.1/A1.2 only and can contain genuine non-target movement. Coverage is the valid comparison-grid percentage; it is distinct from repetition count.

Position is referenced to each model's shoulder. Absolute and initial-posture comparisons are reported separately. All values are in millimetres.

Table A.12: A2 wrist-trajectory RMSE

Side	3D abs.	3D init.	3D cent.	X abs.	Y abs.	Z abs.
P01 L	133.95	225.92	127.19	42.74	115.66	52.33
P01 R	132.80	102.48	66.24	91.53	67.70	68.37
P02 L	119.57	168.26	84.61	73.18	78.46	52.79
P02 R	179.66	245.53	162.78	62.77	146.28	83.31
P06 L	144.58	155.76	119.10	72.58	71.77	102.39
P06 R	196.54	253.87	159.10	111.53	151.97	55.63
P07 L	90.99	113.60	66.53	56.60	48.48	52.19
P07 R	109.42	154.99	96.60	50.82	91.49	31.93

X = right; Y = forward; Z = model up direction. Component RMSE values refer to the absolute comparison. P04 and P05 have no A2 recordings.

Table A.13: A2 terminal-posture repeatability

Side	IMU 3D dispersion	OpenCap 3D dispersion	IMU hold jitter	OpenCap hold jitter
P01 L	15.76	8.30	2.48	3.46
P01 R	23.34	9.44	3.28	2.77
P02 L	16.06	14.57	8.08	8.85
P02 R	20.77	6.80	7.39	6.23
P06 L	19.93	18.56	7.37	4.41
P06 R	15.18	10.67	5.80	2.70
P07 L	17.13	21.20	5.53	8.63
P07 R	32.22	20.15	10.56	11.98

Dispersion describes the spread of mean terminal positions across repetitions. Hold jitter describes within-hold fluctuations. Neither is an independent accuracy measurement against the mouth.

A.5. Test B1

Origin: TO on the sternum. The initial resting wrist position is distinct from the origin. Z follows the gravity-defined vertical direction. All spatial values are in millimetres.

Table A.14: B1 wrist-trajectory RMSE

Side	3D abs.	3D init.	3D cent.	Z abs.	Z init.	Z cent.
P01 L	107.42	83.58	66.61	45.33	21.77	20.87
P01 R †	251.78	726.45	212.44	188.64	586.44	176.23
P02 L	167.58	210.99	143.74	100.73	85.99	58.97
P02 R	147.62	175.55	118.89	87.02	88.47	47.58
P04 L	154.37	183.16	123.21	79.09	83.38	38.82
P04 R	105.81	77.17	54.38	35.20	24.56	18.94
P05 L	182.67	235.43	147.15	105.64	89.84	63.04
P05 R	86.79	116.99	78.32	31.02	23.63	17.65
P06 L	154.87	155.82	94.63	87.98	84.88	55.80
P06 R	148.83	128.60	74.60	58.52	83.63	48.36
P07 L	93.35	108.58	76.69	47.76	39.57	28.41
P07 R	118.18	110.47	82.08	34.30	32.26	25.64

†: P01 right has uncertain temporal alignment and is excluded from the main IMU-MOT summaries. Values describe the full analysed trajectory, not only target holds.

Table A.15: B1 lateral position relative to the model midline (mm)

Side	Chest signed	Chest abs.	Mouth signed	Mouth abs.	Forehead signed	Forehead abs.
P01 L	46.05	46.05	21.07	21.07	-0.03	3.52
P01 R	67.57	67.57	81.56	81.56	32.11	32.11
P02 L	-3.10	3.10	-14.37	14.37	-60.84	60.84
P02 R	-23.84	23.84	-30.54	30.54	-2.27	7.42
P04 L	50.38	50.38	-15.03	15.03	-18.00	18.00
P04 R	13.62	23.46	14.24	14.24	-5.05	5.05
P05 L	-20.27	20.27	-30.46	43.24	-79.40	79.40
P05 R	-17.29	17.29	11.50	12.20	32.87	32.87
P06 L	-12.76	70.88	-54.79	69.05	-49.17	49.17
P06 R	29.31	39.22	25.25	25.25	7.22	35.29
P07 L	3.65	7.87	-0.62	6.08	-12.13	12.30
P07 R	-9.65	30.30	-17.25	17.25	8.68	12.07

Signed = mean of the three hold-mean X values. Abs. = mean of their absolute values, not absolute value of the signed mean. These summaries were calculated from the rounded x_mean_mm values.

Table A.16: B1 external-height agreement on matched sides (mm)

System	Target	n	Mean bias	Mean MAE	Mean RMSE
IMU	Chest	6	-23.78	83.33	85.58
IMU	Forehead	6	10.00	43.89	47.80
IMU	Mouth	6	-10.74	54.49	59.51
MOT	Chest	6	27.56	42.03	45.64
MOT	Forehead	6	19.46	31.48	33.95
MOT	Mouth	6	-6.93	34.36	38.33

Same eleven matched sides from six participants. Sides averaged within participant, then participants averaged with equal weights. These are averages of participant metrics, not errors pooled across samples.

List of Figures

2.1 Experimental sequence of the symmetric bimanual task performed with the UULE: starting position, approaching the object, grasping, and transferring it toward the mouth [14]. 14
2.2 Examples of serious game interfaces developed for the CAR/BiCAR systems: Rehab Basketball, Square Apple, Grabbing Apple, Paper Plane, Round Pizza, Motorcycle, MineCart, and Sakura Flowers [1]. 15

3.1 Modular architecture of the processing pipeline, including NGIMU acquisition, synchronization, kinematic processing, visualization, recording, and analysis. 19
3.2 Schematic positioning of the three NGIMU units on the master side. (Generated with AI) 20
3.3 N-pose, T-pose and F-pose calibration procedures and mirror transformation across the sagittal plane.(Generated with AI) 24
3.4 3D viewer. 27

4.1 Absolute, initial-posture and centred angular RMSE. Bars and error bars show the mean and SD across participants after averaging their complete sides. Black symbols indicate mean centred RMSE. Sample sizes and values are reported in Table 4.2. 41
4.2 P04 right A1.3. Absolute and initial-posture angular comparisons, with IMU-OpenCap differences in the lower panels. RMSE decreases from 38.75° to 9.07°; centred RMSE remains 7.50°. 44
4.3 A2 trajectories for P07 LEFT, the case with the lowest absolute 3D RMSE. The left panel shows the three-dimensional reconstruction and the right panel its forward-upward projection. 45
4.4 P05 right B1. Wrist height relative to TO and the external chest, mouth and forehead references. Shaded bands identify the contact windows. . . . 47

5.1 Bimanual simulation with the right and left arms alternately acting as the master. The virtual slave reproduces the reflected master configuration across the trunk sagittal plane. 50

6.1 Pipeline development towards an IMU-exoskeleton system. 54

List of Tables

2.1 Summary of the main control strategies for robot-assisted upper-limb rehabilitation. 7
2.2 Main sensing modalities used in robotic systems for upper-limb rehabilitation. 10
2.3 Main coordination patterns relevant to bimanual rehabilitation. 13

3.1 Principal evaluation task. 32

4.1 Trial coverage and number of analyzed repetitions 39
4.2 Angular summary for complete blocks. 40
4.3 Isolated-movement RMSE by participant and side 42
4.4 ROM SD in complete blocks 43
4.5 A2 comparisons for all available sides 45
4.6 B1 trajectory RMSE 46

A.1 Group angular agreement (degrees) 58
A.2 Angular agreement: A1.1: shoulder elevation 59
A.3 Excursion and repeatability: A1.1: shoulder elevation 60
A.4 Angular agreement: A1.2: shoulder elevation 61
A.5 Excursion and repeatability: A1.2: shoulder elevation 62
A.6 Angular agreement: A1.3: elbow flexion 63
A.7 Excursion and repeatability: A1.3: elbow flexion 64
A.8 Angular agreement: A2: shoulder elevation 65
A.9 Excursion and repeatability: A2: shoulder elevation 65
A.10 Angular agreement: A2: elbow flexion 66
A.11 Excursion and repeatability: A2: elbow flexion 66
A.12 A2 wrist-trajectory RMSE 67
A.13 A2 terminal-posture repeatability 67
A.14 B1 wrist-trajectory RMSE 68
A.15 B1 lateral position relative to the model midline (mm) 69
A.16 B1 external-height agreement on matched sides (mm) 69